VŠB – Technical University of Ostrava
Faculty of Electrical Engineering and Computer Science
Department of Cybernetics and Biomedical Engineering

Diagnosis of malignant haematopoietic diseases based on the automation of blood microscopic image analysis

Diagnostika maligních onemocnění krvetvorby na základě strojového zpracování mikroskopického obrazu krve

Ostrava 2019 **Bc. Alexandra Bodzás**

VŠB - Technical University of Ostrava
Faculty of Electrical Engineering and Computer Science
Department of Cybernetics and Biomedical Engineering

Diploma Thesis Assignment

Student: **Bc. Alexandra Bodzás**

Study Programme: N2649 Electrical Engineering

Study Branch: 3901T009 Biomedical Engineering

Title: Diagnosis of Malignant Haematopoietic Diseases based on the Automation of Blood Microscopic Image Analysis
Diagnostika maligních onemocnění krvetvorby na základě strojového zpracování mikroskopického obrazu krve

The thesis language: English

Description:

1. Malignant hematopoietic diseases and their manifestations in peripheral blood image.
2. Selection of appropriate software environment for computer processing of the microscopic blood images with possible hematopoietic disease classification.
3. Design of image processing techniques for image segmentation and object detection.
4. Implementation of fundamental algorithms for blood cell classification.
5. Experimental verification of image processing algorithms.
6. Evaluation of results.

References:

[1] PENKA, Miroslav a Eva SLAVÍČKOVÁ. *Hematologie a transfuzní lékařství.* Praha: Grada, 2011. ISBN 978-80-247-3459-0.
[2] AYMAN S. EL-BAZ, RAJENDRA ACHARYA U, ANDREW F. LAINE, JASJIT S. SURI a EDITORS. *Multi modality state-of-the-art medical image segmentation and registration methodologies.* Boston, MA: Springer Science+Business Media, 2011. ISBN 1441981942.
[3] SONKA, Milan, Vaclav HLAVAC a Roger BOYLE. *Image processing, analysis, and machine vision.* New York: Chapman & Hall Computing, 1993. Chapman and Hall computing series. ISBN 0-412-45570-6.
[4] PUTZU, Lorenzo, Giovanni CAOCCI a Cecilia DI RUBERTO. Leucocyte classification for leukaemia detection using image processing techniques. *Artificial Intelligence in Medicine.* 2014, 62(3), 179-191. ISSN 0933-3657. DOI: 10.1016/j.artmed.2014.09.002.
[5] ŠÁLEK, Cyril. Diagnostika a léčba akutních leukemií. *Interní medicína pro praxi.* 2012, 14(10), 366–372. Print ISSN 1212-7299. Dostupné také z: https://www.internimedicina.cz/pdfs/int/2012/10/05.pdf.
[6] PENKA, Miroslav a Eva TESAŘOVÁ. *Hematologie a transfuzní lékařství I.* Praha: Grada, 2011. Print ISBN 978-80-247-3459-0.
[7] *Hematology atlas.* Dostupný z: http://hematologyatlas.com/principalpage.htm.

Extent and terms of a thesis are specified in directions for its elaboration that are opened to the public on the web sites of the faculty.

Supervisor: **doc. Ing. Jan Žídek, CSc.**

Consultant: Ing. Jan Kubíček, Ph.D.

Date of issue: 01.09.2018

Date of submission: 30.04.2019

doc. Ing. Jiří Koziorek, Ph.D.
Head of Department

prof. Ing. Pavel Brandštetter, CSc.
Dean

Declaration

I hereby declare that the present Master thesis was composed by myself and that the work contained herein is my own. I have quoted all the references I have drawn upon.

Alexandra Bodzás

Ostrava, April 26th, 2019

Acknowledgement

In preparation of my Master thesis, I had to take the help and guidance of some respected persons, who deserve my deepest gratitude. Foremost, I would like to express my sincere gratitude to my thesis advisor doc. Ing. Jan Žídek, CSc. for his supervision, special guidance, and encouragement through the development of this thesis. I would also like to expand my deep gratitude to all those who have directly and indirectly guided me in writing this thesis.

Abstract

Leukemia is one of the leading causes of death among human and the prognosis highly depends on the early detection and diagnosis of the disease. In clinical practice, the primary suspicion of the leukemia is determined by the manual microscopic evaluation of peripheral blood smear image. Since this diagnostic method is time-consuming, lacks standardized accuracy and prone to errors due to various human factors, there is a high demand for the automated system, which would minimize the human intervention. The aim of this thesis is to propose a computer-aided leukemia diagnostic system based on image processing and machine learning techniques. To detect and identify the leukemic cells in the blood smear, methodologies such as image preprocessing, image segmentation, features extraction and classification are implemented. The overall automated system achieves recognition rates of 96.53 % by using artificial neural network and 97.92 % by implementing the polynomial SVM classification. The proposed system is successfully implemented in software development environment LabVIEW.

Keywords

Automated leukemia detection, acute leukemia, digital image processing, hematological image analysis, leukemic cells, LabVIEW

Abstrakt

Leukémie patří k hlavním příčinám úmrtí u člověka, přičemž prognóza této nemoci vysoce závisí na její včasné detekci a diagnóze. V klinické praxi je primární podezření na leukémii indikováno prostřednictvím manuálního mikroskopického vyšetření obrazu periferní krve. Vzhledem ke skutečnostem, že je tato diagnostická metoda časově náročná, postrádá standardizované protokoly a je vysoce náchylná k chybám způsobenými lidskými faktory, existuje na trhu velká poptávka po automatizovaném systému, který by byl schopen minimalizovat tento zásah specialistů. Cílem této diplomové práce je navržení automatizovaného, počítačem-řízeného systému založeném na metodách zpracování obrazu a technikách strojového učení. Pro detekci a identifikaci leukemických buněk v krevním nátěru jsou implementovány základní metody pro předzpracování, segmentaci obrazu, extrakci příznaků a klasifikaci. Navržený automatizovaný systém v této práci dosahuje celkové přesností 96.53% použitím metody umělých neuronových sítí a přesnosti 97.92 % použitím metody SVM. Automatizovaný systém pro detekci leukemie je implementován ve vývojovém prostředí LabVIEW.

Klíčová slova

Automatizovaná detekce leukemie, akutní leukemie, digitální zpracování obrazu, analýza hematologických snímků, leukemické buňky, LabVIEW

List of Contents

List of symbols and abbreviations used

RBC – Red blood cell
WBC – White blood cell
HSC – Hemopoietic stem cell
BM – Bone marrow
N/C – Nucleus-cytoplasmatic ratio
AML – Acute myeloid leukemia
ALL – Acute lymphoid leukemia
CML – Chronic myeloid leukemia
CLL – Chronic lymphoid leukemia
OOP – Object-oriented programming
LV – LabVIEW
DIP – Digital image processing
GLCM – Gray level co-occurrence matrix
MAD- Median absolute deviation
SVM – Support vector machine
ANN – Artificial neural network
CNN – Convolutional neural network

List of figures

List of tables

Introduction

The term malignant hematopoietic disease is referred to the excessive and unregulated division of hematological cells. Hematologic malignancies represent the fourth most common cancers and the second leading cause of cancer death worldwide. From a pathophysiological perspective, these malignancies are manifested by the abnormal buildup of cancerous cells which prevent the blood from performing its normal functions. The most common hematological malignancy affecting both adults and children is leukemia. Clinically, leukemia is subdivided into four principal subtypes according to the rapidity of the disease progression and the type of affected white blood cell. To determine the most effective treatment, the accurate diagnosis of the leukemia type is required.

In the diagnosis and treatment of leukemia digital image processing and machine learning techniques play a prominent role. The visual examination of morphological changes in white blood cells of patient's blood is still essential to determine the nature of the leukemic cells. The morphological analysis of peripheral blood smears is often influenced by human factors such as the experience of the hematology specialists or the operator fatigue. Since these high interpersonal differences in human vision could result in non-standardized reports, there is a high demand for a cost-effective and accurate automated system for leukemia screening, which will eliminate human mistakes in the microscopic diagnosis.

The work presented in this thesis is focused on the design and the realization of an algorithm for automated image-based leukemia detection. The methodology presented in this thesis consists of various image processing techniques comprising pre-processing techniques, image segmentation, features extraction and object classification. The proposed automated leukemia detection system is implemented in the software development environment LabVIEW and the application architecture is based on the object-oriented programming paradigm, which ensures the modularity and reusability of the code in such extensive concepts.

The topic of the thesis was chosen on the basis of my experience gained during the studies. Within the professional practice at the department of clinical hematology, I was introduced to the field of the diagnosis and treatment of malignant hematological diseases. Hence I have decided to deal with this issue not only from the medical standpoint but also from a technical point of view. The possibility of automated identification and diagnosis of malignant cells and therefore leukemic diseases via computer vision techniques can save tremendous amounts of time and increase the efficiency of the diagnostics and the research, since the potential human error factor will be suppressed.

1. Blood physiology

Blood is a highly specialized fluid connective tissue which represents the main part of the internal environment of an organism. Blood is a suspension of formed blood elements in extracellular matrix called plasma. Technically it is a transport liquid which carries dissolved substances to all parts of the body. The normal blood pH is restricted to a narrow range between 7.35 and 7.45 and the viscosity is approximately three to four times higher than the viscosity of water.

The primary function of the blood is to transport the materials and cellular waste throughout body. It carries oxygen and carbon dioxide to ensure the exchange of gases between the cells of the body and the blood, provides essential nutrients from the digestive system, transports hormones and removes metabolic waste. Apart from the transport function blood performs a number of specific functions which are listed below.

- Maintenance of homeostasis[1]
- Immune function – performed by white blood cells
- Regulation of the body temperature
- Blood coagulation

The main components of blood include plasma and formed elements that cover blood cells and platelets. Plasma is a non-cellular, yellow colored fluid which forms about 55 % of the total volume. Human plasma is predominantly composed of water (up to 95 % by volume), and contains dissolved substances such as carbon dioxide, glucose, hormones, proteins, mineral salts, fats and vitamins. It serves as a solvent and carrier medium for all nutrients and cellular components. [1] [2]

1.1 Functional morphology of cellular components

The formed elements of blood include two types of blood cells, red blood cells (RBC) and white blood cells (WBC). The most abundant cell type in blood is the red blood cell also called erythrocyte. The primary function of RBC is to carry oxygen from lungs to all body tissues and return carbon dioxide from tissues to the lungs. White blood cells called leukocytes have a lower percentage in blood with a ratio of about 1 WBC to every 600 to 700 erythrocyte. They take part in a most important role in phagocytosis[2] and make up the majority of the immune system, and therefore in defense against foreign substances and various types of infections. The detailed morphology of the blood components is discussed in the next chapters. [1]

[1] Self-regulating process by which biological system tend to maintain constant internal environment

[2] Process by which certain cells called phagocytes engulfs particulate matter such as microorganisms, cells, ect.

1.1.1 Erythrocytes

The shape of erythrocytes is a flattened, circular, biconcave disc. The circumference of the cell is approximately three times thicker than the central part. Plasma membrane of a mature RBC is composed of lipid bilayer which is a semipermeable, self-assembly arrangement of phosphates and lipid molecules, transmembrane proteins and cytoskeletal network. This skeleton comprising mainly polymeric spectrin and actin (cytoskeletal proteins) molecules and the unique shape of the cell gives the erythrocyte resilience and flexibility. This allows the cells to stretch and bend as they squeeze while traversing the circulatory system and to spring back to original shapes.

RBC lacks nucleus and mitochondria to store greater amount of hemoglobin that is responsible for gas transportation via simple diffusion. Hemoglobin is a predominant protein consisted of protein chains called globin and iron containing pigment hem, which gives a blood its characteristic color. Each hemoglobin molecule consists of four globins, which are bounded to one hem and has the ability to bind four molecules of oxygen. As a result of missing nucleus the lifespan of erythrocytes is limited to 120 days. [3] [4]

1.1.2 Leukocytes

Leukocytes commonly known as white blood cells are the only formed elements which are complete cells including nucleus and organelles. Unlike red blood cells they are independently motile and have considerably shorter circulating time. In case of acute infection the lifespan of leukocytes is shortened to a few days or hours depending on the type of cell. Whereas RBCs circulate within the blood vessels, WBCs leave the bloodstream to perform their immune and defensive functions in body's tissues.

White blood cells are highly differentiated for their specialized functions. On the basis of their appearance, they are divided into two groups according the amount of highly visible granules in cytoplasm. Granular leukocytes (granulocytes) contain enzyme-containing granules which are released during inflections and allergic reactions and comprise neutrophils, eosinophils, and basophils. Agranular leucocytes (agranulocytes) are distinguished from granulocytes by nucleus shape (usually round without lobes) and absent or less obvious granules. The agranulocytes include monocytes that mature into macrophages with ability to phagocytose and lymphocytes defined by high nuclear cytoplasmic ratio[3] (N/C). The morphology of basic classes of leukocytes is shown in Figure 1 and the detailed overview of the cell's function is listed in the next section.

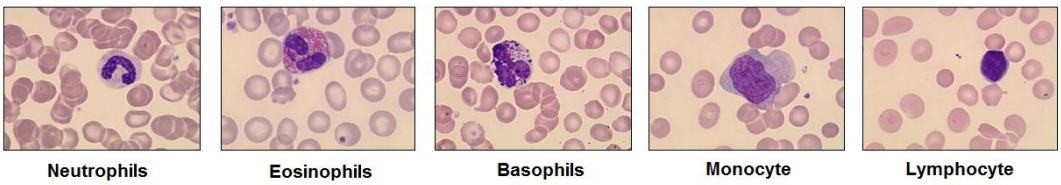

Figure 1: Manifestation of elemental leukocytes in normal peripheral blood smear. [*1*]

[3] The relative ratio of the nucleus to the cytoplasm of the cell.

- Neutrophils – produce antimicrobial substances and enzymes that help destruct or inhibit the growth of pathogens during infection, inflammation and tissue injury

- Eosinophils – have beneficial role in defense against parasitic infestations or during immediate allergic reactions and autoimmune diseases

- Basophils – incite immediate allergic reactions releasing histamine which increase the flow of blood to injured tissue via dilating the blood vessels and secrete heparin that acts primarily as an anticoagulant

- Monocytes – differentiate into macrophages that ingest and process foreign material, microorganisms, dead cells and cellular debris

- Lymphocytes – provide the body's immune response mechanism and include natural killer cells (recognize and kill cancer cells or cells infected with virus), B-cells (secrete antibodies that attack bacteria, viruses, and toxins) and T-cells (produce signaling molecules called cytokines which suppress or regulate immune responses) [1] [4] [5]

1.1.3 Thrombocytes

Thrombocytes also called platelets are irregular, colorless, disc-shaped elements derived from the fragmentation of larger bone marrow cell called megakaryocyte. These fragments are bounded by membrane and in the center have a group of basophilic granules, which contain substances important for the clot-promoting activity. Like erythrocytes they are anucleated and incapable of cell division. On the surface platelets contain adhesive proteins which allow them to adhere to each other and to stick to breaks in the blood vessel.

The main function of platelets is to maintain the hemostatic process which prevents blood loss during vascular injury. The bleeding is arrested by formation of adherent mass of thrombocytes forming temporary platelet plugs. Upon activation, the intracellular granules secret vasoconstrictors causing vascular spasm in ruptured blood vessel and highly active procoagulatory mediators that promote blood clotting. [5]

1.2 Hematopoiesis

Mature blood cells have a relatively short life span therefore they must be continuously replaced with new cells. The process of continuous development and formation of cellular components of blood is called hematopoiesis. Each formed blood element is derived from the pluripotent hemopoietic stem cell (HSC), which have the ability to develop into all types of precursors of blood cells. During cell division at least some of daughter cells remain as HSCs with self-renewal capability (long-termed HSCs) while the short-termed HSCs can follow any of the other lineage differentiation that leads to the production of multi-potential and lineage-committed cells preceding

maturity. This generation of cellular diversity maintains the stem pool size and ensures the constant tissue regeneration. Classically, HSCs are thought to differentiate into two major branches, the lymphoid lineage producing lymphoid cells which include T-cells, B-cells and natural killers and the myeloid lineage which differentiate into granulocytes, monocytes, megakaryocytes and erythrocytes. The simplified scheme of hematopoiesis is demonstrated in Figure 2. [6]

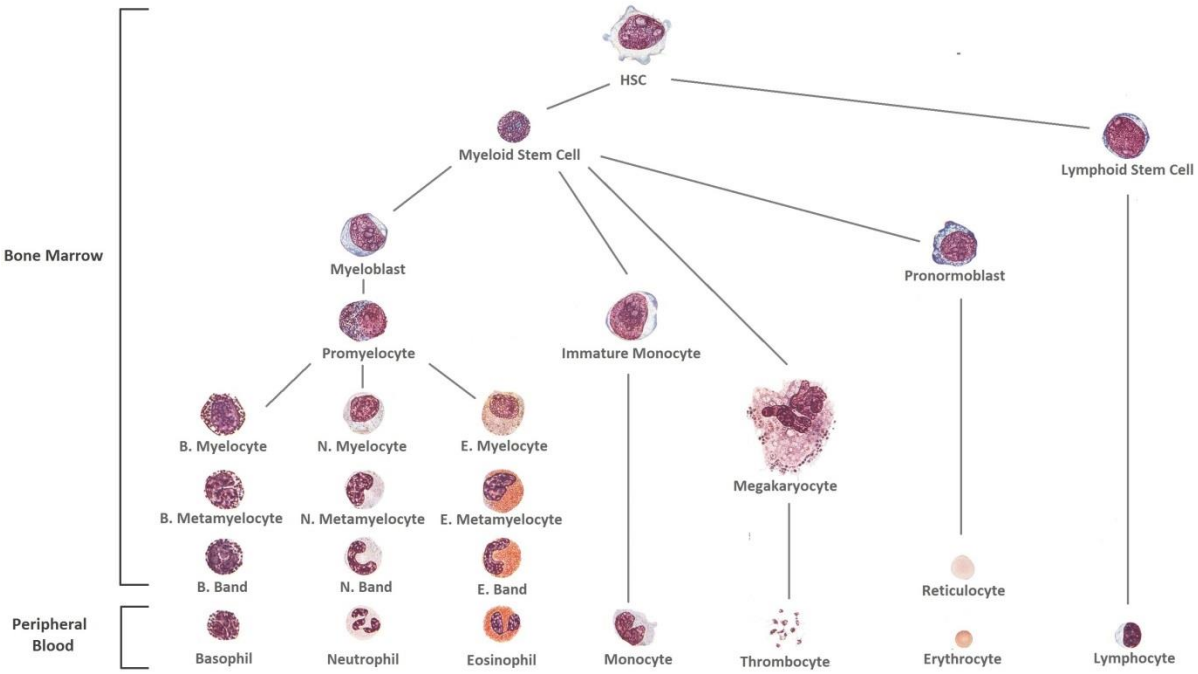

Figure 2: Development of human blood cells [*2*]

In the human adult hematopoiesis occurs within the hematopoietic system that comprises organs and tissues such as the bone marrow (BM), spleen, thymus and lymph nodes. Bone marrow produces erythrocytes, platelets and most white blood cells while the lymphoid cells mature in spleen, thymus, and lymph nodes. In case of hematological disorders hematopoiesis is often observed under certain pathological conditions in spleen, liver, lungs, urogenital system or skin. The process of hematopoiesis is driven by growth and transcription factors, which manage the development of specific mature lineages. [6]

2. Hematopoietic malignancies

Hematological malignancies are disorders that arise as a result of unregulated clonal proliferation[4] of blood cells. According to the affected type of cell, hematopoietic malignancies are divided into two groups. The lymphoid neoplasia which develop from the malignant transformation of normal lymphoid blood cells at various stages of differentiation and the myeloid neoplasia that arise from the myeloid lineage including precursor cells to erythrocytes, thrombocytes and granular leukocytes. In compliance with the *WHO Classification of Tumours of Haematopoietic and Lymphoid Tissues* the myeloid neoplasms are classified into nine main sections comprising e.g. myeloproliferative neoplasm, myelodysplastic syndromes, mastocytosis, acute myeloid leukemia or leukemia of ambiguous lineage. Lymphoid malignancies cover a wide spectrum of disorders which are categorized into precursor lymphoid neoplasms, mature B-cell neoplasms, mature T-cell and NK-cell neoplasms, Hodgkin lymphomas and histiocytic and dendritic cell neoplasms. [7]

2.1 Diagnostic techniques of hematologic malignancies

The laboratory diagnosis and monitoring of hematological malignancies is complex and requires a wide range of information derived from various modalities including morphology, cytochemistry, cell phenotyping, cytogenetics, and molecular genetics. Despite advances in hematology automation and application of molecular techniques, the morphology still remains the key frontline diagnostic technique. Using a light microscopy for the morphological examination of peripheral blood smears and bone marrow aspirates may permit the definitive diagnosis or at least provide a provisional diagnosis that determines the further, more advanced investigation methods. Imaging is done with a 10× magnification at first to find the most suitable area and to note red and white blood cell densities. The detailed leukocyte analysis is performed afterward with a 60× to 100× oil-immersion objective. The morphological examination of peripheral blood smear can be also used for manual blood cell counting, however, due to high interpersonal differences in cell recognition this procedure is largely replaced by automated cell counters. Abnormalities on a complete blood cell count and WBC differential[5] may be considered as the first indication of a hematological neoplasm and generally precede peripheral blood staining. [8] [9]

Apart from the previous conventional diagnostic techniques cytochemistry plays an important role in routine hematology laboratory practice. These supplementary cytochemical staining methods allows effective visualization of certain enzymes and chemical substances within the cells. Each developing cell produces specific substances which can be detected while using certain synthesized or organic dyes. Localization of these chemical biomarkers provides an important clue to the cell lineage and its detailed classification. Since the cellular morphology alone sometimes can be misleading or even confusing, it is inevitable to evaluate genetic biomarkers (see Chapters 2.1.1 and 2.1.2). [10]

[4] Rapid and excessive growth or reproduction of cells, parts, tissues, etc.

[5] Blood test which determines the proportions of different types of leukocytes in the blood.

2.1.1 Immunophenotyping

In the last decade flow cytometric immunophenotyping remains an indispensable utility for the diagnostic and prognostic stratification, the disease subtype classification, and the monitoring of hematological malignancies. Immunophenotyping is a method used for the analysis of heterogeneous populations of cells for the purpose of detecting the presence or absence of WBC antigens. Antigens, also known as markers are superficial or intracellular functional membrane proteins that could be unique to specific cell types in certain combinations. These markers are identified by special fluorescently-conjugated antibody reagents that bind to specific antigens. As the fluorescing cell interacts with the laser beam, the fluorochrome in dye excites and the scattered light is detected. The acquired signals are processed and displayed in histogram or scatter plot.

Currently, there is a large panel of monoclonal antibodies[6] which detect different markers on normal and leukemic cells of various lineages and differentiation. The selection of the antibodies is primarily based on the morphological and cytochemical findings. According to the recognized antigen, the antibodies are grouped and identified under a cluster designation number (CD). Phenotypic aberrancies are documented in many hematologic neoplasms, including lymphomas, plasma cell neoplasms, chronic lymphoid leukemias, acute leukemias, myelodysplastic syndromes or myeloproliferative disorders. In these clinical cases immunophenotyping provide a sensitive screen for the presence of hematologic malignancy. [11] [12]

2.1.2 Clinical and molecular cytogenetics

Application of cytogenetic and molecular genetic techniques in clinical diagnosis can provide invaluable additional therapeutic and prognostic information. The study of chromosomal defects and gene mutations in hematological malignancies helps the specialist assess the prognosis of the patient, select the most appropriate therapy or detect the relapses of the disease. Conventional cytogenetic analysis enables detection of all microscopically visible chromosome aberrations involving rearrangements within chromosomes or both gain and loss of chromosome segments. This method is based on the numerical and structural microscopic analysis of metaphase chromosomes. For the purpose of arresting the cells in the metaphase, in which chromosomes are in their most condensed and microscopically visible stage, clinicians use mitosis inhibitors. To be considered relevant, the identified chromosome aberrations must be present in at least of two metaphase cells of an identical structural abnormality. Usually, the slides are prepared from living leukocytes from the peripheral blood or bone marrow. [13] [14]

Conventional cytogenetic analysis could not provide sufficient outcomes, due to the fact that it can be performed only on dividing cells. Therefore, the study must be complemented with more sophisticated molecular methods. Molecular cytogenetics comprises a large set of techniques that enable identifying chromosome aberrations at the level of the DNA sequence. For the detection and localization of DNA or RNA sequences the fluorescence in situ hybridization (FISH) laboratory technique is most commonly used. FISH technique relies on exposing the chromosome to small isolated DNA fragments called probes, which are labeled with a fluorescent dye. Under optimized

[6] Antibodies designed to identify and bind to specific receptors found on the cells.

conditions, probes bind to specific complementary sequences of DNA, which can be observed through the use of a fluorescence microscope. Compared to standard cytogenetics, the FISH test provide chromosome analysis in non-dividing cells and can identify genetic abnormalities that are too small to be seen under a conventional microscope. [10] [14]

2.2 Leukemia

Leukemia is a general term describing a group of malignant disorders that are manifested by the tumorous proliferation of certain types of WBCs in the bone marrow. The malignancy varies according the type of leukemia from non-malignant to highly aggressive forms. The pathological WBCs also called blasts or leukemia cells are not fully developed and do not perform their defensive function. Blasts suppress normal hematopoiesis and crowed out the normal blood elements in human body causing difficulties with fighting infections, controlling bleeding or transporting oxygen. Morphologically, blasts can often be distinguished from mature forms by having a large nucleus with finely dispersed chromatin and one or more prominent nucleoli manifested by small pale areas. The cytoplasm is moderate and usually basophilic without granules. Morphological differences between normal peripheral blood smear and blood with excessive buildup of immature blasts is demonstrated in Figure 3. Clinically leukemia is divided in two ways. The first division is based on the rapidity of the disease progression. Acute leukemia develops quickly. Rapidly Increasing blasts are very immature and incapable of normal functions, while chronic leukemia progress slowly over time and pathological cells are more mature and carry out some of their normal function. Due to the higher maturity of the blast in chronic leukemia, the early symptoms may be mild or even unnoticed. The other type of leukemia sub classification depends on the type of affected WBCs. This divides leukemia into myeloid and lymphoid. Combining these two classifications provides the four most common subtypes of leukemia, the acute lymphocytic leukemia (ALL), chronic lymphocytic leukemia (CLL), acute myeloid leukemia (AML) and chronic myeloid leukemia (CML). Incidence of leukemia varies considerably by geography and the specific subtype and is generally higher in males, with a global male to female ratio of 1.4. [15]

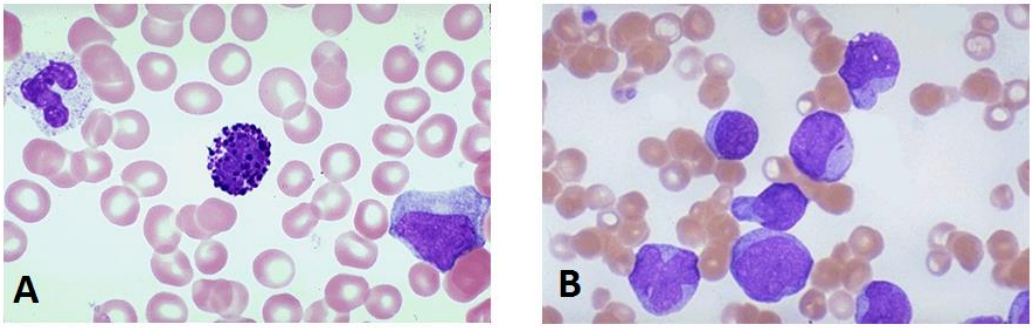

Figure 3: Microscopic images of peripheral blood: (A) Normal blood [*3*], (B) Acute leukemia [*4*]

Currently there are two major systems established for classification of acute types of leukemia into particular subtypes. The French American British (FAB) classification system solely based on the morphologic and cytochemical features of peripheral blood and bone marrow aspirates, and the

extended World Health Organization (WHO) system. FAB classification which was developed in the 1970s did not reflect fully the clinical diversity of the disease therefore it has been largely replaced by WHO classification system which takes into account genetic, immunophenotypic or other clinical features of the cell. The FAB model for leukemia classification categorizes AML into eight subtypes (M0 through M7) and ALL into three subtypes namely L1, L2 and L3. The subsequent chapters consider only the FAB model for leukemia classification. [16]

However leukemia is the most common type of blood cancer with around 350 000 new cases diagnosed worldwide each year, the five-year survival rate for leukemia has more than quadrupled since 1960s. Especially childhood ALL represents one of the most dramatic successes in cancer treatment with almost 90% survival rate. The prognosis of disease depends upon several factors including primarily the patient's age, presence of high number of leukocytes, type of leukemia or the extent to which a cancer has developed by growing and spreading. In general, children younger than two years and adults aged over 70 have a poorer prognosis. The overall global survival rates are demonstrated in Table 1. [17]

Table 1: Five-year relative survival rate for major leukemia types (2009-2014) [18]

Type of leukemia	Five-year survival rate
AML	27.4 % overall, 66.4 % for children and adolescent younger than 15
ALL	71.0 % overall, over 90 % for children and adolescent younger than 15
CML	68.0 %
CLL	86.2 %

2.2.1 Acute myeloid leukemia

AML also known as acute myelocytic leukemia, acute granulocytic leukemia or acute non-lymphocytic leukemia is the most common type of acute leukemia occurring in adults (median age at diagnosis is 67 years). It accounts approximately for 70 % of all acute leukemia diagnosis with an incidence of 3.5 new cases per 100 000 people per year. AML is clinically a group of clonal neoplasms that arise from malignant transformation of hematopoietic precursor cells. The chromosomal rearrangements and multiple gene mutations results in excessive production of poorly differentiated myeloblasts which are not capable to mature into more differentiated cell types. Irritated hematopoietic cells proliferate primarily in bone marrow, where they interfere with the normal hemopoietic process and subsequently penetrate into the bloodstream, therefore the other organs can be infiltrated. [19] [20]

The diagnosis of AML is defined by the presence of at least 20 % of myeloid blasts in bone marrow compared to less than 5 % which is considered to be normal. The disease can be diagnosed as well by the observation of chromosomal abnormalities occurring in specific types of myeloid leukemia even if the blast percentage is lower. FAB classification model divides AML into eight subtypes based

on the morphology of blasts after routine staining. Subtypes M0 through M5 starts in immature forms of leukocytes while M6 shows primarily erythroid differentiation with dysplastic and M7 evolve from primitive megakaryocyte precursor. The morphological features of leukemic cells in peripheral blood smear are summarized in Table 2. [19]

Table 2: Morphological features of AML subtypes based on the FAB classification [21]

Morphology	Classification	Name	Description
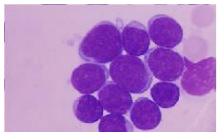	M0	Undifferentiated AML	medium sized blasts, round to oval nucleus with fine chromatin and non-granular basophilic cytoplasm
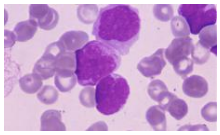	M1	AML without maturation	medium sized blasts with high N/C, round nucleus with immature chromatin
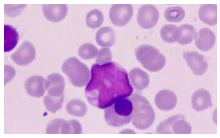	M2	AML with maturation	small to medium sized blasts with high N/C, rounded nucleus with scattered immature chromatin and with one or more nucleoli
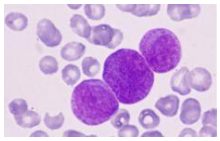	M3	Acute promyelocytic leukemia	rich azurophilic granulation, irregular or bilobed nucleus, cytoplasm with elongated crystalline inclusions
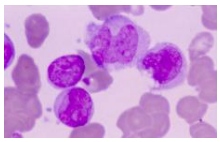	M4	Acute myelomonocytic leukemia	large blasts with usually prominent nucleoli, nucleus rounded or irregular
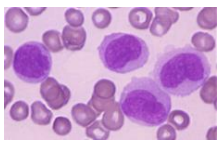	M5	Acute monocytic leukemia	large blasts with round nucleus and large basophilic cytoplasm containing auer rods[7]

[7] Clumps of azurophilic granular inclusions in the cytoplasm

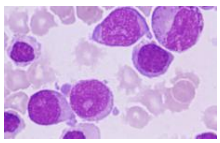	M6	Acute erythroblastic leukemia	medium sized erythroblasts with extreme dysplastic features including giant forms and cytoplasmic buds or vacuoles
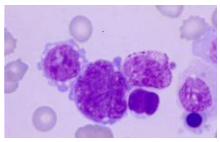	M7	Acute megakaryoblastic leukemia	highly immature blasts with eccentric nucleus, reticulated chromatin and non-granular cytoplasm, presence of giant platelets

Patients with AML usually present with symptoms resulting from bone marrow failure manifested by abnormally low concentration of erythrocytes, platelets and some types of leukocytes or symptoms related to organ infiltration (i.e. enlargement of spleen and liver, swollen and bleeding gums, seizures, bone or joint pain, respiratory distress). [22]

2.2.2 Acute lymphoid leukemia

ALL is the second most common acute leukemia in adults and the most common malignancy in children, accounting for one third of all pediatric cancers. The estimated worldwide annual incidence of adult acute lymphoblastic leukemia is about one new case per 100 000 people, whereas in children the incident rate is almost four times higher. ALL is a malignant disease caused by the chromosomal mutation and genetic alterations of hematopoietic stem cells of the lymphoid lineage. The excessive production of lymphoblasts, which do not develop into mature infection-fighting B lymphocytes or T lymphocytes, crowed out normal cells in bone marrow and usually metastases to other essential organs such as lymph nodes, liver, spleen or CNS. Overall 75 % of cases develop from precursors of the B-cell lineage. [23] [24]

According to FAB classification there are described three major subtypes of ALL: Ll, L2 and L3 (shown in Table 3). The most significant difference between the subtype L1 and L2 is the size of the leukemic cells and the heterogeneity of the ALL-L2. Subtype L3 is associated with a specific chromosome abnormality and significantly larger vacuolation compared to other types of leukemia. Since the morphological classification does not provide high clinical and prognostic relevance, especially for subtypes L1 and L2, the system has been largely replaced by the WHO classification. This method based on the immunophenotyping analysis replaced morphologic terms of FAB classification L1 and L2 with an immunologic classification comprising precursor-B and precursor-T ALL which are further sub classified by cytogenetic abnormalities. [25]

Table 3: Morphological features of ALL subtypes based on the FAB classification [26]

Morphology	Classification	Name	Description
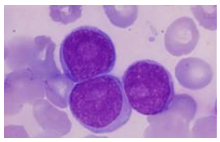	L1	Lymphoblastic leukemia with homogenous structure	small blasts with high N/C, scanty cytoplasm, regular nucleus and chromatin with barely visible nucleoli
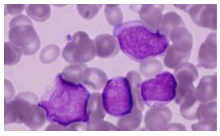	L2	Lymphoblastic leukemia with varied structure	blasts of variable size and N/C, large nucleoli, nucleus irregular with heterogeneous lacy chromatin
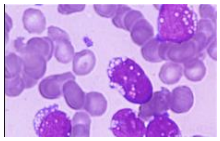	L3	Burkitt's leukemia	large blasts with prominent nucleoli and stippled nuclear chromatin, cytoplasm amply vacuolated

Clinically the features of ALL sufficiently differ from the myeloid type of leukemia therefore separate diagnostic and treatment protocols are required. Many symptoms of ALL are vague and nonspecific and overlap with the symptoms of AML, particularly those related to deficiency of normal blood elements. Even though this leukemia remains the leading cause of cancer-related deaths in pediatrics , the long-term survival rate approaches 90 % in children. The long-term remission in adults is much more modest and accounts for 30 to 40 percent. [23]

2.2.3 Chronic types of leukemia

Chronic leukemia includes a broad spectrum of malignant hematopoietic disorders. Their clinical manifestation, prognosis, and treatment strategies differ widely depending on the type of leukemia. Compared to acute leukemia, the chronic phase has a slow progression which frequently does not appear for a long period or even remains unnoticed. The malignant transformation of cells takes place in a later stage of the hematopoietic process and therefore the tumor cells are more mature than in the acute forms of the disease. However the cells appear normal, they are unable to maintain normal physiologic functions. The continuous increment of leukemic cells in the body is caused by the higher lifespan of abnormal cells even though the proliferation is much slower. Based on the affected cell line chronical leukemias are classified into two main groups, the chronic lymphocytic leukemia, which results mainly in the buildup of B lymphocytes and the chronic myelogenous leukemia affecting granulocytes. The morphological features with the detailed description of both types of chronic leukemia are shown in Table 4. [27]

Table 4: Morphological differences between CML and CLL in peripheral blood smear. [*5*] [*6*]

CML	CLL
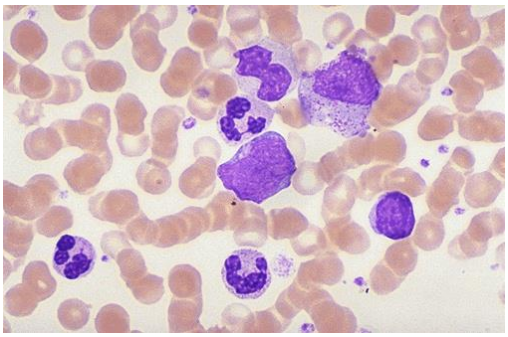	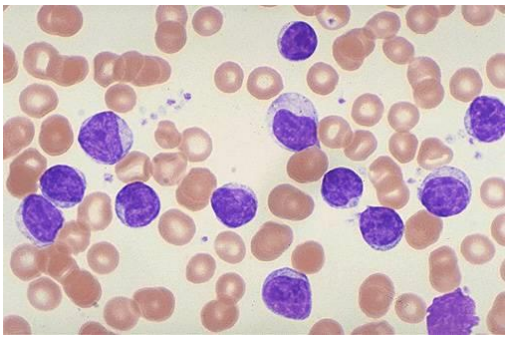
Presence of whole spectrum of myeloid cells including small myeloblasts, segmented neutrophilic granulocytes and monocytes of different degrees of maturity. Blast Phase of CML: excess blasts with different values of N/C, slightly irregular nucleus with fine chromatin and moderately basophilic cytoplasm. [28]	Lymphocytes slightly larger than normal small lymphocytes, scant cytoplasm with round to slightly irregular nucleus containing chromatin clumps, small or ambiguous nucleoli. Presence of "smudge" cells (fragile neoplastic cells which loss their form during slide preparation). [29]

CML has historically been a triphasic disease. Without treatment, there is a gradual transition from the chronic to more aggressive phase called the accelerated phase which can culminate in the blast crisis. By definition, patients in the blastic phase present with 30 or more percent of blasts in peripheral blood and 50 or more percent in BM. After being diagnosed, there is 6% chance of the disease progression to a next phase. In this case patients have a less favorable prognosis with the median survival rate between 7 and 11 months. Cases with initially present accelerated phase or blast crisis have significantly higher relative survival rates in comparison with a continuous progression of the disease. Most patients with CLL or aggressive phases of CML presents with weakness, extreme fatigue, weight loss and progressive marrow failure. [26]

3. Programming environment selection

Digital image processing is a rapidly evolving technology, especially in the fields of computer vision, information science, robotics, or in medical diagnostics. This concept is concerned primarily with enhancing the image quality and extracting useful information from the image. The crucial designing problem during the image processing system development is, on the one hand, the requirement of the highly run-time efficient code with a low-level hardware interface and on the other hand, a platform-independent implementation providing all data types and extended functions for image processing. For the purpose of acquiring desired results in machine vision and image processing, many development environments can be used. Often they are complemented with extensive libraries which carry out the image analysis. The most convenient programming environments and toolkits for image processing are mathematically oriented software such as Matlab, open source image processing library *OpenCV* and *Vision development module* designed for LabVIEW.

OpenCV (short for Open Source Computer Vision Library) was designed for computational efficiency with a focus on real-time applications. The library contains a comprehensive set of optimized algorithms related to computer vision and machine learning. The algorithms can be moreover widely applied for face detection and recognition, tracking moving objects, gesture recognition, 3D model extraction, etc. OpenCV supports a broad spectrum of programming languages like C, C++, Python and Java, and is available on different platforms including Windows, Android or Linux. [30]

In comparison with OpenCV, Matlab has a built-in *Image Processing Toolbox* which supports common automatic image processing workflow. These tools help to create applications for image processing, analysis, visualization or develop more complex algorithms performing image segmentation or object classification. Matlab is an interpreted language which negatively affects its performance, especially in terms of the computational speed. The major advantage of using Matlab against other text-based programming languages is the fact that Matlab operates on a simple syntax format which is easier to implement. For the purpose of designing and implementing the practical part of the thesis, the development environment LabVIEW complemented with the vision library is used. [31]

3.1 LabVIEW

Laboratory Virtual Instrument Engineering Workbench or LabVIEW (LV) for short is a system-design platform and software development environment created by National Instruments, which is a worldwide leader in the area of virtual instrumentation. In comparison with the conventional text-based programming languages that use instructions to determine the program execution, LabVIEW, creates programs using a graphical notation. The source code of the program, in this case, consists of connected functional nodes that make up the particular functional parts. These nodes can either be sinks, sources or processing blocks to the information. Created LabVIEW

programs are called virtual instruments or VIs since their appearance, operation and behavior imitate real devices in their physical forms.

The programming paradigm used in LabVIEW is based on the principles of dataflow programming. The order in which code executes is determined by the structure of a graphical block diagram and therefore the way that data flows across wires through the nodes on the block diagram. The execution of nodes can be performed only in case that all required inputs become available. Thus allow simultaneous processing of tasks. To determine the order of the execution among multiple available nodes, LabVIEW uses a process called arbitrary interleaving. This makes multitasking code diagrams easier to design.

Apart from a comprehensive set of tools for data acquisition, analysis or visualization, LabVIEW comprises a broad spectrum of application-specific libraries e.g., for communication, SW validation, machine vision, real-time signals processing, or database connectivity. This software development environment is therefore suitable not only for the signal measurement and analysis but also for the programming of more complex technological processes such as robotic systems. [32]

3.1.1 Object oriented programming in LabVIEW

Object-oriented programming (OOP) refers to a type of software design in which programmers break a system down into discrete, independent entities called objects. Objects also defined as classes group together properties (data) and methods (tasks and functions) into one self-contained unit with own role and responsibility. This encapsulation ensures the modularity of the code and keeps the data safe from external interference. The relationships between different classes are represented by the inheritance. The inheritance enables new class to acquire properties of the base class (also called super class or parent class). The derived classes usually termed as subclasses or a child classes automatically take over the same information and can perform the same actions along with their own additional properties and methods. Using the concepts of inheritance helps organize classes into a basic control hierarchy. It allows easier modification or extension of the program without affecting the overall application. A key mechanism of OOP is the polymorphism, which supports the capability of data to be processed in more than one form, depending on the type of object that invokes the function.

Object oriented programming in LabVIEW differs in many aspects from other OOP approaches in other functional languages. In comparison with text-based programming languages, LabVIEW has an ultimate ancestor class managing all objects and automatic data mutation that enables users to retrieve old data even if the class has been edited. Unlike C++, LV does not support multiple inheritance, which gives the class the possibility to inherit characteristics and features from multiple parent classes. Using OOP in LabVIEW encourages cleaner interfaces between particular segments of the code. This reduces the possibility of introducing errors into not related parts of code during the maintenance and makes debugging easier. The development of classes in LabVIEW is supported by *NI GOOP Development Suite* that extends the capabilities of NI LabVIEW built-in object-oriented features. [33]

3.1.2 Vision development module

National Instruments *Vision Development Module* provides principal support for the development of industrial machine vision and scientific imaging applications in LabVIEW. This software package includes a robust set of image processing algorithms for binary, complex number, grayscale and color image processing and visualization. The high-level programming library involves an extensive set of complete optimized functions comprising for instance filters, arithmetic operations, morphology calculations, 3D imaging, pattern matching, particle analysis, object classification algorithms and other methods for image enhancement and manipulation. The module also features a license for *Vision Acquisition Software* driver which is necessary for image acquiring, displaying and logging data from a large number of different camera types. This module is also equipped with an interactive environment called *Vision Assistant* that gives developers a quick prototype of vision applications without programming. [34]

4. Image processing in computer vision

Computer vision is an interdisciplinary field which deals with the integration and automation of a wide range of processes used for visual perception. The initial goal of computer vision is to enable machines to see and interpret the visual world as the human visual system can do. As a scientific discipline, it is closely linked with the theory and technology of building artificial systems. Within the past decade, computer vision systems are used in various types of environments including agriculture, automotive, biometrics, robotics, security and surveillance, or healthcare. Many of these applications involve tasks which require working in a hostile environment, using large databases, or either demands a high rate of processing. The most frequent application in industrial and clinical practice concern object recognition, object measuring and tracking, defect detection, or automatic driving. This is mainly performed by image processing and machine learning techniques. [35]

Image processing, or more specifically digital image processing (DIP), focuses on developing a digital system which is able to perform processing operations on a digital image. It can be thought of as a transformation of an image into a new desired image. This can be done by using efficient algorithms. Interest in DIP methods stems from two principal application tasks, the improvement of pictorial information for human interpretation and the processing of image data for storage or transmission. The task of digital image processing can be broken up into three computerized processes (low-, mid- and high-level process). Generally, the aim of low-level processing is to improve the visual quality of the input image by simple processing tasks such as image enhancement and restoration. The middle layer acts as an interface between the low-level image analysis and high-level interpretation layers. It involves tasks which primarily perform feature extraction, pattern recognition, and image segmentation functions. Unlike low layer, the mid-level processing outputs are usually in a symbolic form representing the extracted attributes such as position, edges, or contours of the particular portions. Finally, the higher level image processing techniques use a combination of medium layer functions to perform cognitive functions associated with human vision such as object interpretation. [36]

4.1 Representation of a digital image

In the field of image processing, two-dimensional unitary transforms play an important role. The transformation between different image domains is realized by basis functions. Each discrete function *f (x,y)* in a space domain can be expressed as a linear combination of selected orthogonal basis functions by the relation

$$f\ (x,y) = \sum_{u}^{X-1} \sum_{v}^{Y-1} F\ (u,v) * \varphi_{u,v}\ (x,y) \qquad (1)$$

where *x, y* are the coordinates in the transform domain, *F (u, v)* is a function returning the value of an image (intensity, color, number of electrons) at coordinates *u, v* and $\varphi_{u,v}$ *(x,y)* is the basis function for the transform.

Different basis functions enable to extract particular color spaces of the image, determine the spectrum of frequency components, or reconstruct the image from the frequency domain. For the purpose of the real image discretization from the three-dimensional domain, the Dirac delta function is used. The Dirac delta function is regarded as a generalized function or distribution which presumes to satisfy the following conditions:

$$\delta_n(x,y) = \begin{cases} \infty & x,y = 0 \\ 0 & otherwise \end{cases} \tag{2}$$

$$\iint_{-\infty}^{+\infty} \delta(x,y)dxdy = 1 \tag{3}$$

The digital image is therefore defined by two-dimensional discretized function *f(x,y)* where *x* and *y* are the horizontal and vertical spatial coordinates. The amplitude of each element of the 2-d array represents the intensity values of the image at the appropriate coordinates. To represent color images, separate color components are specified. Each pixel in the image is usually a three-dimensional vector represented by the intensities of particular color spaces. [37] [36]

$$f(x,y) = \begin{bmatrix} r(x,y) \\ g(x,y) \\ b(x,y) \end{bmatrix} \tag{4}$$

The graphical representation of the function of a two-dimensional grayscale image is demonstrated in Figure 4.

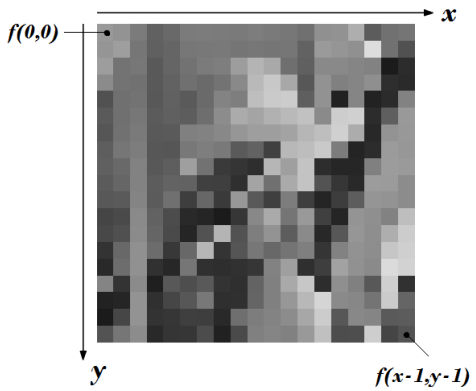

Figure 4: Representation of a grayscale digital image

4.1.1 Color models

The appearance of the real-world objects is based on the optical characteristics of a certain object, the reflected light, and human perception. Generally, colors are regarded as electromagnetic waves, which are identified by their wavelengths. The visible spectrum, which can be detected by the human eye, occupies a very small portion of the electromagnetic spectrum with a range of between 390nm (violet) and 720nm (red).

A color model is an abstract mathematical model which visualizes the color spectrum as a multidimensional model. Most color models are usually three dimensional and can therefore be depicted as 3D shapes. In specific cases, they can be more than three-dimensional such as the RGBA model which is complemented by the alpha channel representing the opacity value of the color. The appropriate selection of the color model can significantly improve the performance of image processing, especially regarding the image segmentation techniques. In the following, the most prevalent color models are presented.

- **RGB**

The RGB is one of the most used color spaces, especially for 8-bit digital images. Each pixel value in the RGB model is represented by the pairwise sum of the intensity values of primary colors (red, blue and green). This additive model is usually depicted as a three-dimensional color cube in which the three primary colors form the coordinate axis. Each point in the cube represents a specific color on the RGB scale (see Figure 5).

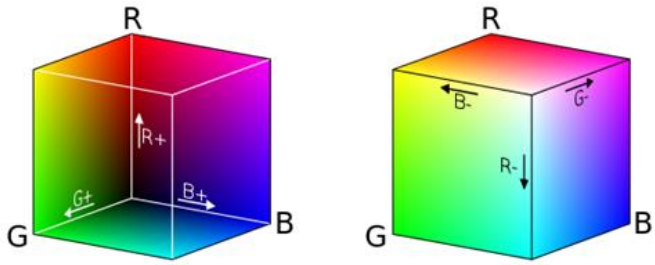

Figure 5: The RGB unit cube. Points along the main diagonal present with grayscale values from black at the origin (0, 0, 0) to white at point (1, 1, 1). [*7*]

- **CMYK**

In comparison with RGB, the CMYK color model (Figure 6) is a subtractive system, where each color space is subtracted to reduce the reflected color spectrum. It is the standard color model used in offset printing where the whole range of colors is achieved by overlapping tints cyan, magenta, yellow and key black, which is added to produce the true black.

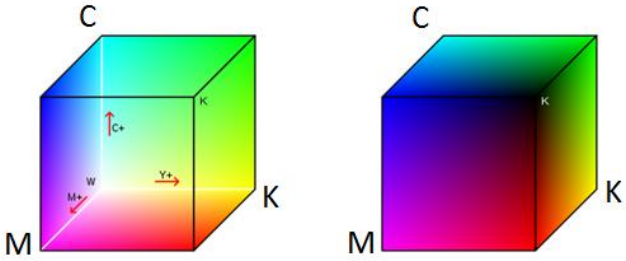

Figure 6: Spatial representation of CMYK color model. [*8*]

- **HSV**

The HSV color model belongs to human-orientated spaces, which transform the RGB system into dimensions that are more closely aligned to human perception of colors. Therefore this model is broadly used in artificial vision systems as a powerful tool in digital image processing algorithms. The system is composed by three components, the hue, that describes the actual pure color, the saturation expressing the purity of the color, and the value representing the brightness or the intensity of the light. Hence this model is also known as HSB that replace the value dimension with brightness.

In comparison with RGB, which is defined by cuboidal coordinates, the HSV model is based on cylindrical or conical coordinates, where the hue represents the circular part of the cone or the cylinder, the saturation is determined by the radius, and the value is the height of the object. The three-dimensional conical formation of the HSV system is demonstrated in Figure 7. Beside the HSV there are two color systems which closely relate to this model, the HSL (hue, saturation, and luminescence) and HSI (hue, saturation, intensity) color model. [38]

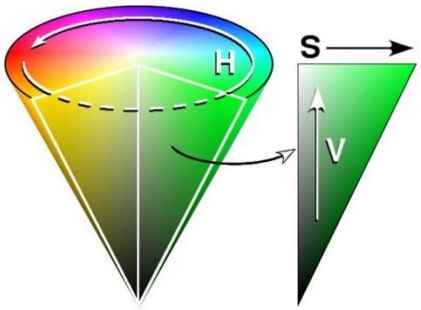

Figure 7: HSV color model in a cone representation. [*9*]

4.2 Low level image processing techniques

Low-level image processing methods play a key part in computer vision, as they enable the extraction of essential descriptions from the image. Generally, the goal of the low-level processing is to attain the highest possible resolution and the resilience to noise or other degradations. This chapter will introduce the fundamental image processing tasks performing image enhancement and noise removal.

4.2.1 Pixel-based image enhancement

Image enhancement techniques comprise a broad spectrum of operations at the lowest level of abstraction. The main aim of the image enhancement is to improve the quality and the information content of the original image for the future automated image processing. The commonly-used enhancement techniques include contrast enhancement, brightness correction, geometric transformations, histogram processing, and variety of filters.

The pixel-based processing methods are based only on the intensity values of single pixels. Each new pixel value depends on the transformation of the corresponding pixel value of the input image. This transformation function is represented as a pixel or point operator and can be defined in the following form

$$g\,(x,y) = \varphi\,\{\,f\,(x,y)\,\} \tag{5}$$

where *f(x,y)* is the original image and φ is the transformation which is applied on the original image to obtain the processed image *g(x,y)*. The detailed overview of selected point-based enhancement techniques is described in the next chapters. [37]

4.2.1.1 Color space transformations

The translation between color spaces is used for various reasons such as, reducing the size of the image, reducing the complexity of subsequent processing, obtaining the specific information, or for aesthetic intents. The most common color conversion is the translation of the color image to grayscale. Color-to-grayscale conversion performs a reduction of the three-dimensional color model into a single dimension. Although the transformations use approximations in order to preserve the most important color qualities, the converted grayscale image may lose some information such as contrasts, sharpness, shadows or the structure of the color image.

The simplest approach to carry out the grayscale conversion is based on neglecting of the chrominance channels and taking a luminance channel as a grayscale representation. In practice, the standard and more accurate conversion method is the Luminance algorithm, which approximates the image gradient to the human vision perception. This approach prevents from loss of discriminative information by using equal contribution of particular color channels. Each pixel value is therefore computed by the relation [39]

$$I = 0.299 * R + 0.587 * G + 0.114 * B \quad (6)$$

4.2.1.2 Gama correction

Gamma correction denotes a simplest single point operation which provides the compensation of the transfer characteristic of an input and output and maps them to uniform intensity space. It performs a nonlinear brightness adjustment based on the exponential gamma function. In simple terms the brightness for each pixel intensity values is increased or decreased by the following relation

$$g\,(x,y) = f\,(x,y)^{\gamma} \quad (7)$$

The original purpose of the gamma correction was the compensation of CRT monitors non-linear response to the input. Since they were not able to amplify the input signal themselves, the gamma encoding adjusts the image and redistributes tonal levels closer to the perception of human vision. [40]

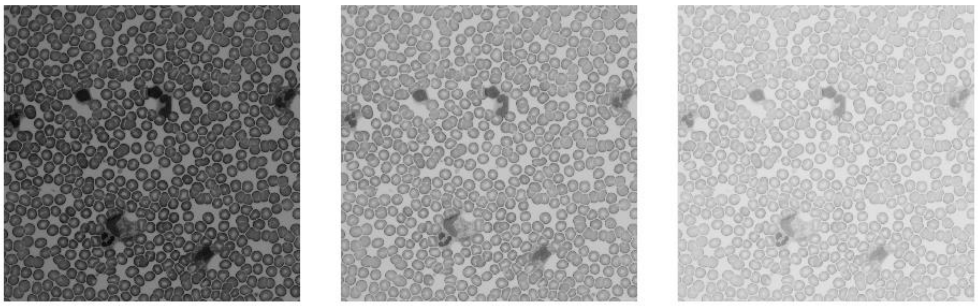

Figure 8: Nonlinear mapping using gamma correction with γ = 2.5, γ = 1, γ = 0.5 (Left to right).

4.2.1.3 Histogram equalization

Histogram equalization is a widely used technique for contrast enhancement of the image. The histogram of a digital image is an accurate representation of the distribution of its intensity levels in the range [0, L-1], where L is the number of available discrete intensity levels. The distribution is a discrete function which associates to each intensity level, the number of pixel with the corresponding intensity. For an 8-bit grayscale image the histogram will display 256 numbers representing the distribution of pixels amongst the particular intensity values.

To perform the enhancement, the cumulative histogram has to be constructed. In probability and statistics, the cumulative distribution function is defined as a function that gives the probability that a continuous random variable is less than or equal to the argument of that function. The probability that a pixel has the intensity *I* equal or lower than x is computed by the following formula

$$cdf(x) = \sum_{i=0}^{j} I_i \tag{8}$$

Intuitively, the final histogram equalization tries to set the brightest pixels to white, the darkest pixels to black and similarly rescale the remaining pixels. This rescaling is performed by the transformation of the original intensity distribution for the purpose of capturing all intensity distribution. The new intensity values for each intensity levels are therefore calculated by the following equation

$$g\,(x) = \frac{cdf(x) - cdf(min)}{MN - cdf(min)}\,(L-1) \tag{9}$$

where *g(x)* is a new value for the old pixel with the value *x*, *cdf(min)* is the least non-zero value element of cumulative distribution function, *M,N* represents the size of the picture and *L* is the number of maximum intensity levels. Figure 9 illustrates histogram equalization using the exact histogram algorithm. [40] [43]

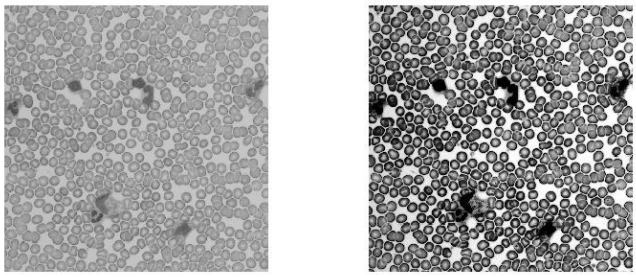

Figure 9: Comparison of the original image (left) with the image after histogram equalization (right).

4.2.1.4 Geometric transformations

Geometric transformations modify the spatial relationship between pixels in the image. Each discrete pixel position in the source image is mapped to a point in a new coordinate system via vector transformation function (see Figure 10). A geometric transformation usually refers to a linear combination of translation, scaling, shearing and rotation operations. These cases of linear 2-d geometric transformations are called as affine transformations. Generally, affine transformations preserve collinearity, which means that all points are lying on a same line before and after the transformation and do not change the ratios of distance. Application of an affine transformation to an image provides the correction of a perspective distortion, mostly caused by remote sensing.

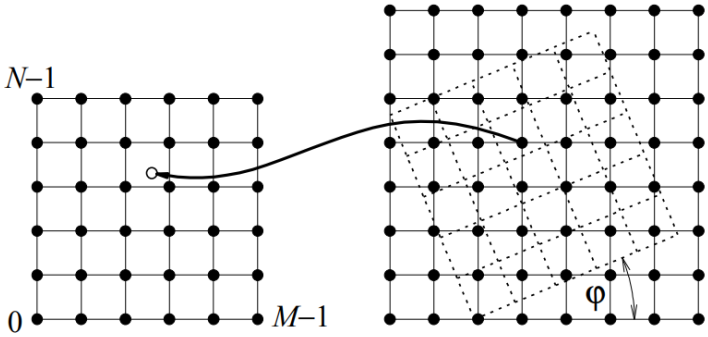

Figure 10: Affine transformation of an image – rotation. [10]

In practice, the transform combinations are usually described in terms of matrix operations which use homogeneous coordinates. These coordinates enable all affine operations to be expressed as a matrix multiplication.

$$\begin{bmatrix} x' \\ y' \\ 1 \end{bmatrix} = \begin{bmatrix} a_{11} & a_{12} & b_1 \\ a_{21} & a_{22} & b_2 \\ 0 & 0 & 1 \end{bmatrix} \begin{bmatrix} x \\ y \\ 1 \end{bmatrix} \tag{10}$$

where *(x',y')* are the coordinates where the point *(x,y)* is mapped and the coefficients a_{11}–a_{22} correspond to a rotation of an image and coefficients b_1,b_2 carry out the translation. Figure 11 shows the transformation matrices for the basic geometric operations performed on the image.

$$\begin{bmatrix} a_{11} & 0 & 0 \\ 0 & a_{22} & 0 \\ 0 & 0 & 1 \end{bmatrix} \qquad \begin{bmatrix} \cos\varphi & -\sin\varphi & 0 \\ \sin\varphi & -\cos\varphi & 0 \\ 0 & 0 & 1 \end{bmatrix} \qquad \begin{bmatrix} 0 & 0 & b_1 \\ 0 & 0 & b_2 \\ 0 & 0 & 1 \end{bmatrix}$$

Figure 11: Left to right: Image scaling, image rotation by φ, translation by coefficients b_1 and b_2.

Let assume that images *f(x, y)* and *g(x, y)* are discrete. Then all points of the output image *g(x, y)* can be mapped by the relation (10) and for each point x, y is determined the corresponding position in the input image. The value of the intensity is then taken from the input image. While the pixels of an input image reside on the rectangular grid with integer coordinates, the transformation produces non-integer pixel locations. To assign the intensity values to intermediate points of the output image, the interpolation methods can be used. The most commonly used interpolation in practice is the bilinear interpolation, which computes the pixel value as a weighted function of the four nearest pixels in integer positions (x_0,y_0), (x_1,y_0), (x_0,y_1), and (x_1,y_1). [40] [37]

4.2.2 Spatial domain filtering

Filtering belongs to techniques used for modifying and enhancing an image. The image processing operations implemented with filtering include mainly image smoothing, sharpening, and edge enhancement. Filtration in a spatial domain is accomplished through an operation called discrete convolution. It is basically a mathematical operation combining two functions, where each value in the output is expressed as a summation of input values multiplied by a set of weighting coefficients. The value of the current pixel therefore depends on both itself and neighboring pixels. The matrix of weights is called the convolution kernel, also known as the filter, mask or template.

The convolution is generally regarded as an application of an operator *O* that transforms an input function *f(x,y)* to an output function *g(x,y)* through a linear operation. To describe the system by the convolution, the applied operator has to be linear and shift-invariant, which means that pixels can be expressed as a linear combination of its neighbors and the same operation is performed for each pixel.

$$g\,(x,y) = \mathrm{O}\{\,f\,(x,y)\,\} \tag{11}$$

Let's assume the convolution operator in a discrete state space and a convolution mask as a Dirac delta function. By application of a linear and shift-invariant operator, the output image can be expressed in the following form

$$g\,(x,y) = \sum_{x}^{X-1}\sum_{y}^{Y-1} \mathrm{O}\{\,\delta(x-a,y-b)\} \tag{12}$$

In case that delta function is the input, the resulting output of the linear system will be the impulse response *h(x,y)*, or more descriptively for images, the point spread function. Knowing the impulse response, of the system is the key point to the complete prediction of the system behavior and for the determination of the output for any given input. The convolution is then given as a multiplication of the input function with the impulse response through the whole image as follows.

$$g\,(x,y) = \sum_{x}^{X-1}\sum_{y}^{Y-1} f\,(x,y) * h\,(x-a,y-b) \tag{13}$$

The convolution kernel is usually a square odd sized matrix with a center and the smallest meaningful size being 3x3. Most of the commonly used masks are derived as a known impulse response in a frequency domain and converted into a spatial domain by reverse Fourier transform. Depending upon the weighting coefficients the operations are classified into low pass filtering and high pass filtering. The concept of low-pass filters is to remove higher frequency content for the purpose of image blurring and noise reduction, while the sharpening spatial high-pass filters highlight and enhance the details in the image. Figure 12 demonstrates the example of effects achieved by the application of different convolution kernels. [36] [37]

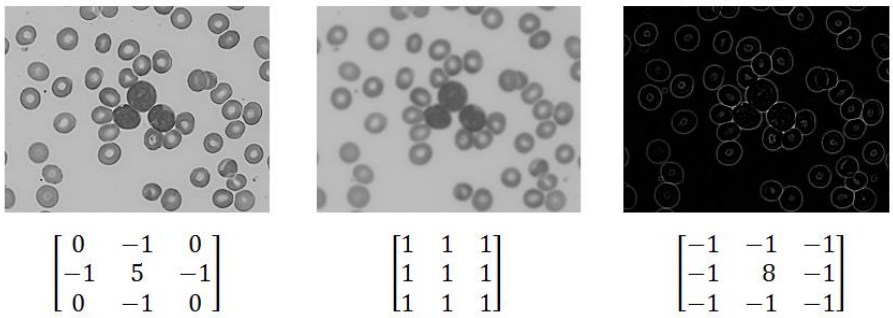

$$\begin{bmatrix} 0 & -1 & 0 \\ -1 & 5 & -1 \\ 0 & -1 & 0 \end{bmatrix} \quad \begin{bmatrix} 1 & 1 & 1 \\ 1 & 1 & 1 \\ 1 & 1 & 1 \end{bmatrix} \quad \begin{bmatrix} -1 & -1 & -1 \\ -1 & 8 & -1 \\ -1 & -1 & -1 \end{bmatrix}$$

Figure 12: Convolution masks performing image sharpening, blurring and edge enhancement.

4.2.3 Mathematical morphology

The morphologic operations are typically defined by set-theoretic concepts and include shape oriented operations that preserve the essential shape characteristics of an image and eliminate the imperfections in its structure. Initially, the technique was only applicable to the binary image, which can be considered as an image in which the image function at each point assumes one of two possible discrete values (0 and 1).

The most important parameter of the morphological operator is the structuring element, sometimes called kernel. Basically, it is a set of point coordinates that are mostly much smaller than the image and is essential for the determination of the effect of a certain applied operator. The structuring element is translated to each pixel position and the new value is obtained on a basis of the comparison of the element with the corresponding underlying image pixel.

The principal application of the morphology is the extraction of useful components in the representation and description of the shape. The often used morphological operations contain algorithms for the extraction of boundaries, extraction of connected components, the convex hull algorithm, the region filling and the skeleton of the region. [36]

4.2.3.1 Dilatation and erosion

Dilatation and erosion are the fundamental algorithms in morphological image processing. In fact, many of the morphological algorithms are based on these primitive functions. Let B be a given binary image and S the structuring element. The $S_{x,y}$ denotes the sub-image resulted from the translation of the structuring element with its beginning within the coordinates (x, y) in the original image. The dilatation D and erosion E are then defined by the expressions

$$E = B \oplus S = \{(x, y) \mid S_{x,y} \subseteq B\} \tag{14}$$

$$D = B \ominus S = \{(x, y) \mid S_{x,y} \cap B \neq \emptyset\} \tag{15}$$

Dilation allows objects to expand and is basically used to fill holes and connect disjoint objects, while erosion causes object to lose its size by etching away their boundaries. This removes the noisy elements in the picture. [36]

4.2.3.2 Hit or miss transformation

The hit or miss transform is another basic binary morphological tool for the shape identification and template matching. As the other morphological operators, hit or miss transform is performed by translating the origin of the structuring element to all points in the image. It is derived by using erosion operation and unlike the previous morphological operations, the structuring element, in this case, is constituted by a pair of elements. If B is an image to be probed, A^c is the complement of the image and S_1, S_2 are the hit and miss patterns representing the single structuring elements for the object and the background, then the hit or miss operation is defined as the

$$B \otimes S = (A \ominus S_1) \cap [A^c \ominus S_2] \tag{14}$$

The hit or miss transform assigns the object value (1) to the pixel underneath the origin of the structuring element only if the foreground and background pixels in the structuring element exactly match to the foreground and background pixels in the image. Otherwise, the pixel is set to the background value (0). The example of an application of the basic morphological operations with the used structural elements is shown in figure 13. [36] [41]

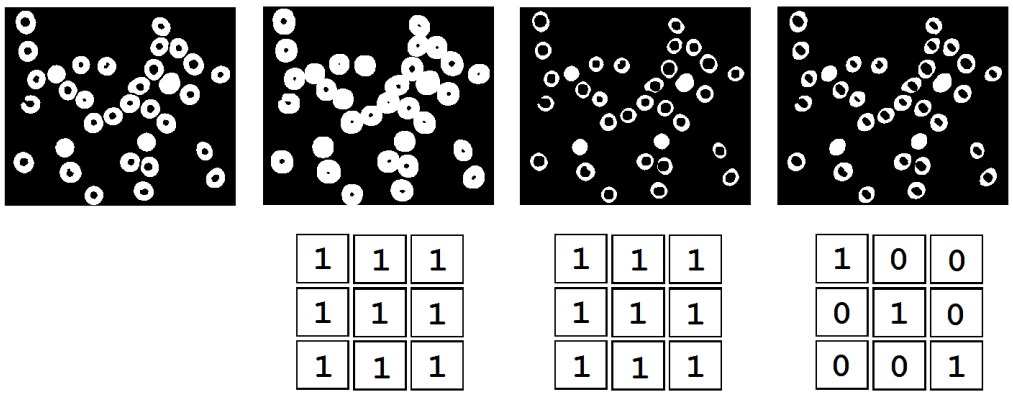

Figure 13: Application of morphological operations: original image, erosion, dilatation, hit or miss transform (left to right).

4.3 Image segmentation techniques

Segmentation has become a prominent task in image processing and computer vision and plays a pivotal role in further image analysis. It is mainly concerned with extracting particular meaningful areas from the images. Basically, these mid-level image processing techniques simplify the image by its subdivision into easily analyzable parts with similar features and attributes. Image segmentation techniques are based on two principal properties of intensity values of the pixels, the discontinuity, and the similarity. The first approach is based on the abrupt changes in the intensity representing the edges of the objects, while the second approach partitions an image into regions with similar properties. The techniques based on the similarity of the pixels are commonly known as region-based segmentation methods and include region growing, thresholding techniques and region merging and splitting algorithms. Image segmentation is also a useful tool, especially in image compression and object recognition, as the processing of the whole image may be in these types of application inefficient. [36]

4.3.1 Thresholding based method

Threshold segmentation method is one of the most commonly used segmentation techniques in region-based segmentation. It is one of the simplest approaches to segment an image based on the intensity value of each pixel. This technique classifies pixels into two categories, the object points and the background. This separation is achieved by the definition of the threshold value *T*. Then any point for which the value of the image function $f(x, y) \leq T$ is called an object point, otherwise, the point is set to the background or vice versa (see equation 15). The effect of using different threshold values is demonstrated in Figure 14.

$$g\,(x,y) = \begin{cases} 0 & if\ f(x,y) > T \\ f(x,y) & if\ f(x,y) \leq T \end{cases} \tag{15}$$

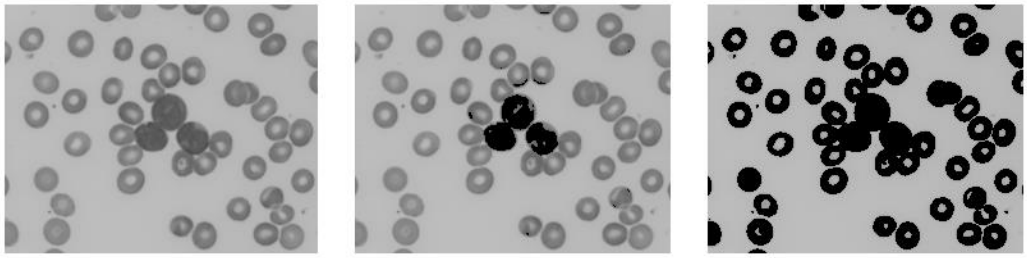

Figure 14: Global thresholding method using different values of threshold.

Thresholding can be distinguished into global threshold method and local threshold method. The global thresholding is in most cases implemented when the differences between foreground and background objects are very distinct. The separation of the objects is therefore solely based on a single threshold value. Some most commonly used global threshold segmentation methods are the interclass variance method (Otsu) that selects the threshold by maximizing the variance between classes, the entropy-based thresholding method, the minimum error method, the simple statistical method and etc.

On the other hand, the local thresholding, also called adaptive thresholding, uses multiple threshold values that vary over the image depending on the local characteristic of different target regions. These techniques determinate the threshold value automatically on the basis of the minimum and maximum mean methods. The biggest advantage over the other technique is the simplicity of the calculations and the fast operation speed. [36] [37]

4.3.2 Region-growing method

The region-growing method is a procedure which groups pixels or sub-regions into larger regions on the basis of specific predefined conditions. The segmentation is realized by selection of an initial set of small areas, called seed pixels which are merged with the surrounding pixels according to mutual similarity. The region is iteratively grown from the seed pixel by comparing and allocating the neighboring pixels. The similarity is determined by the difference between the intensity value of the pixel and the mean intensity of the whole region. The growth of the region stops only if the difference between the mean of the region and the intensity value of the pixel becomes larger than a defined threshold. However this segmentation technique is simple and provides good boundary information and segmentation results, a key problem is the possibility of incorrect region chaining caused by misleading join between the neighboring pixels. This can be observed particularly in noisy data. The coordinates of the seed pixels are usually given or selected randomly. To improve the effectiveness and the accuracy of this technique some automate seed selection algorithms are proposed. Usually, these algorithms are based on extracting features, regions or edges. [36]

4.3.3 Edge Detection

The most important information of the image can be found in the edges, which are local discontinuities in intensity values of the image. Since edges typically correspond to object boundaries or changes in surface orientation, extraction of these features is extensively used in image segmentation. Term edge detection refers to a process of identifying and locating distinct abruptions in the image. In general, there are many edge detection methods founded on different principles which include error minimization, wavelet transformation, fuzzy logic, objective function maximization, etc. The majority of various methods may be grouped into two categories, the edge detection using the first-order derivative and the detection using the second-order derivative.

- **First-order derivative**

The first order derivative detectors, or also called gradient detectors are based on the various approximation of a two-dimensional gradient, which is regarded as the partial derivative in the vertical and horizontal direction. A value of the partial derivatives $\partial f/\partial x$ and $\partial f/\partial y$ need to be computed at every pixel in the image. The gradient operator of an image $f(x,y)$ at the coordinates x, y is defined as a vector in the following form

$$\nabla f(x,y) = \begin{bmatrix} G_X \\ G_y \end{bmatrix} = \begin{bmatrix} \partial f(x,y) \,/\, \partial x \\ \partial f(x,y) \,/\, \partial y \end{bmatrix} \tag{16}$$

The properties of the particular intensity discontinuities in digital images are given by the magnitude, which provides information about the strength of the edge, and the direction of the gradient. The magnitude |∇f| and the direction α of an increase of the gradient at location *x, y* are given by the relations (17) and (18). The computed angle is measured with respect to the horizontal axis and the direction of the edge at specific coordinates is perpendicular to the direction of the gradient vector at that point.

$$|\nabla f(x,y)| = \sqrt{G_x^2 + G_y^2} \tag{17}$$

$$\alpha\,(x,y) = \arctan\left(\frac{G_y}{G_x}\right) \tag{18}$$

The most frequently used edge detectors based on a single derivative are Sobel, Prewitt, Roberts, and Canny edge operator. These operators are based on convolving the image with a small, separable filter in the horizontal and vertical direction. Using operators with smaller masks may lead to inaccurate edge points, especially in noisy images. These unwanted inaccuracies are mostly alleviated by the extension of the size of the neighborhood.

Out of the mentioned algorithms, Canny edge detection is considered as an optimal method for the edge localization and detection. In comparison with the other edge detection operators, Canny uses a multi-stage algorithm that includes besides the gradient calculation also algorithms for the image smoothing, non-maxima suppression which suppress points that do not lie in important edges or hysteresis thresholding determining the relevant edges. The comparison of using different edge detecting filters is shown in Figure 15. [42] [36]

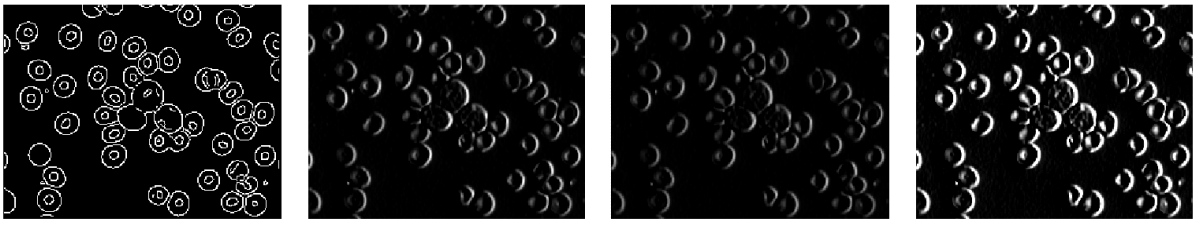

Figure 15: Edge Detection operator. From Left to right: Canny, Sobel, Prewit, Kirsch.

- **Second-order derivative**

The edge detection technique discussed in the previous section is solely based on the convolution of the image with different kernels, without taking into account the noise and the characteristics of the edges. The second-order derivative algorithms are often applied to the images that have been smoothed by application of the low-pass filter. The main principle of this method is to search for zero crossings in the second derivative of the image for the purpose of detecting edges. Finding the zero crossing can identify the exact location of the gradual transition of intensity from

dark to the bright region and vice-versa. The second-order derivative of the intensity is actually the Laplacian which can be expressed for a two-dimensional image function as

$$\nabla^2 f(x,y) = \frac{\partial^2 f(x,y)}{\partial x^2} + \frac{\partial^2 f(x,y)}{\partial y^2} \tag{19}$$

This method is usually rather used for extracting some secondary information then for the edge detection. The main reasons are the unacceptably high sensitivity to the present noise, the occurrence of double edges produced by the magnitude and the inability to detect the direction of the edge. The operators using the zero crossing approach comprise except the Laplacian, the Laplacian of Gaussian and the Difference of Gaussian operator. Despite the disadvantages of this technique, it still remains as a useful tool to determine, whether the point lies on the darker side or the bright side.

Although edges in zero crossing are much thinner than the gradient edges and the fine details are much more enhanced, due to noise reduction capabilities and higher computational complexity of this method, the gradient based edge finding techniques are still used more frequently in segmentation algorithms. [42] [36]

4.3.4 Watershed algorithm

Watershed segmentation technique, also denoted as morphological watershed, embodies different concepts of segmentation included in previous chapters. It provides a complementary approach to the object segmentation, especially in cases when the segmenting objects are touching each other. The main idea of the morphological watershed is to associate a specific zone to each regional minima of an image. The watershed then determines the boundaries which separates the particular zones. The basic concept of this algorithm is based on the visualization of an image into a three-dimensional topographic representation, which includes three types of points: points that belong to a regional minimum, points at which a drops would fall with certainty to a single minimum (catchment basins), and points at which drops would be equally likely to fall to more than one minimum (watershed or divide lines).

One of the possible algorithmic approaches to compute the watershed of the image can be realized by the simulated immersion. Each local minimum in the image can be regarded as a surface with a hole that is immersed out into water. The entire surface is then flooded from the bellow by letting water rise through the catchment basins at a uniform rate. This flooding is at each level achieved by planar distance propagation. During this process basins are about to overflow and may merge with each other. To avoid this event, the conceptual dams are built on the points of the surrounding ridge line, where flood would merge. The process is stopped by reaching the highest peak in the surface, where catchment basins corresponds to image regions and ridgelines or watershed lines relate to region boundaries. [36]

Using a standard morphological watershed transformation on the image degraded by noise can often lead to over-segmented image. To decrease the over-segmentation, several techniques based on image preprocessing and postprocessing have been proposed. The most popular techniques comprise marker-controlled watershed segmentation, region merging methods, edge enhancement and noise reduction methods based on partial differential equations, or wavelet techniques. Figure 16 demonstrates the segmentation of the image after the application of the standard watershed algorithm.

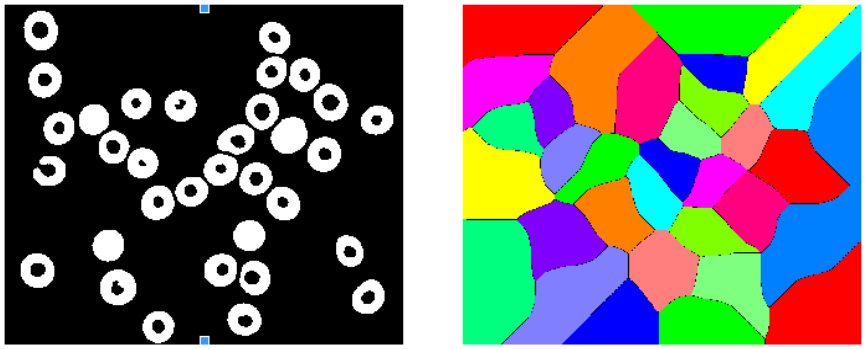

Figure 16: Result of applying the watershed segmentation algorithm to a binary image.

The biggest advantages of using the watershed transformation are the provision of closed contours after the segmentation and a low computation speed in comparison with other segmentation techniques.

4.4 High-level image processing

High level image processing covers the most complex and extensive field of the computer vision. This task involves object recognition and scene interpretation by performing cognitive functions normally associated with human vision. Hence for the purpose of performing such tasks, artificial intelligence methods are widely used. In addition, high level image processing encompasses processes, which extract high-dimensional attributes from images in order to produce numerical or symbolic information that is processed to help recognize the individual objects. The information from the input data is usually extracted in the way that the amount of the kept data is reduced while the essential information is preserved. There are typically two different approaches to perform the object identification, the model-based recognition and learning-based recognition.

The goal of the model-based recognition, also known as unsupervised learning, is to model a structure or distribution in order to obtain useful information about the data. This approach group unsorted information that is neither classified nor labeled to several clusters on the basis of their similarities. Majority of used unsupervised learning algorithms belong to the clustering method. This technique divides the population or data points into a number of clusters in such a way that data points belonging to the same group have similar properties, while samples in different clusters are highly dissimilar. The similarity between the particular data points is usually quantified by a distance metric. Some of the most common algorithms used in unsupervised learning include K-means, self-organizing maps, autoencoder, or principal component analysis.

Unlike model-based methods, supervised learning requires training data containing both inputs and desired outputs. The input and output data are labelled for the classification to provide supervision during the learning process. The basic concept is to find a certain structure or relations in the input data, which allows effective and correct classification of the outputs. In general, the learning cycle consist of a few distinct phases. In the first phase, the training data are propagated through the model producing output responds. These responds are afterwards compared with the assigned label of the corresponding training data in order to estimate the model's error, which is used to solve the given problem by adjusting model’s parameters. The most widely used algorithms for performing supervised learning include naive Bayes, random forests, logistic regression, support vector machines and artificial neural networks.

Since model based methods are not suitable and reliable tools in a discipline of image classification, supervised learning techniques are more likely used for this purpose. The selected supervised techniques for the blood cell classification are discussed in more detail in Chapters 5.5.1 and 5.5.2. The following chapters present the practical application of the research methodologies and a proposed image processing based system for detecting leukemic cells.

5 Microscopic blood image processing

Visual microscopic examination is often used as a first step in the process of leukemia diagnosis. It performs quantitative as well as qualitative analysis of microscopic blood smear images. Since this methodology is solely based on the human visual perception and rely on the personal experience of domain experts it has a limited statistical reliability. To reduce the human intervention and increase the reliability of leukemic cells detection, automatic analysis systems are under development. These computer-based diagnostic systems usually combine image processing and machine learning techniques. The general sequence of steps in automatic leukemia detection systems is illustrated in figure 17. These steps include image preprocessing of acquired blood smear images, segmentation process for the purpose of isolating WBCs and features extraction for extracting useful components from the region of interest followed by the classification process.

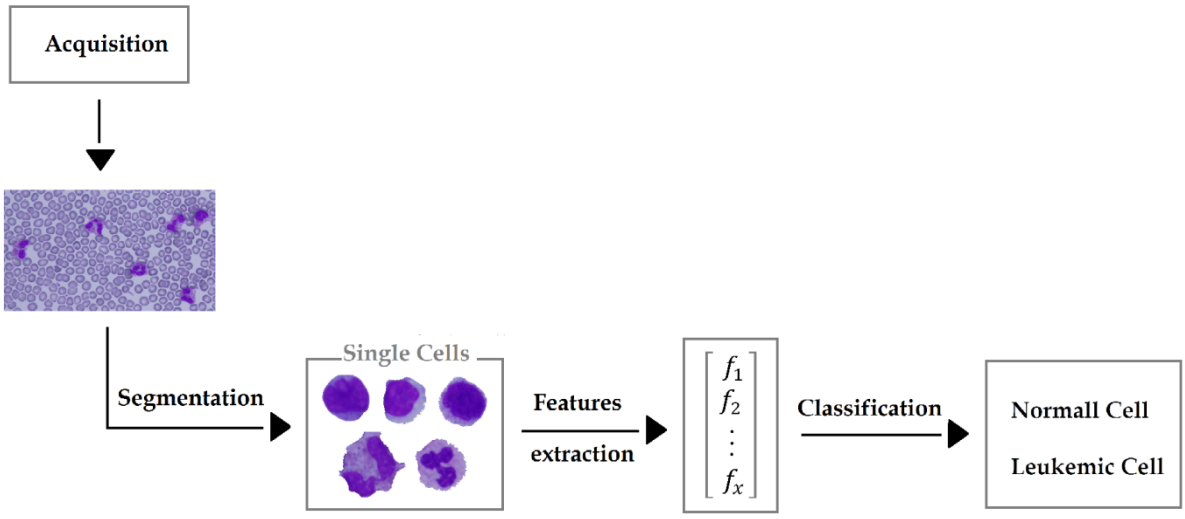

Figure 17: The automatic leukemia diagnostic system phases

5.1 Blood smear image acquisition

The demonstrated procedure in figure 17 is realized on the image database comprising 31 peripheral blood smear slides of different patients with acute leukemia and normal diagnosis. Since the leucocytes on a prepared blood smears are distributed unevenly with the predominance of large leukocytes on the border and smaller cells in the center, systematic data acquisition is required. The better evaluation of the diagnosis is therefore ensured by obtaining at least two microscopic images per each patient. During the image acquisition process the meander system was carried out, which allows to capture microscopic images from different consecutive locations. The slides were collected at the hematological laboratories of FNO Ostrava and performed on blood films stained with Giemsa stain to visualize the cell components abnormalities.

.

Blood smear images are captured by Olympus CX43 microscope under 50× zoom with oil immersion objective lens and with an effective magnification of 500×. All microscopic images in the

database are saved in the bmp format with the 24 bit color depth and resolution equal to 4080 × 3072 pixels.

5.2 Preprocessing

During the process of data acquisition, many variable factors, such as blood film thickness, staining time, illumination adjustment or present film defects lead to undesirable visual artifacts or different color distribution among particular digitized blood smear images. To deal with the potential artifacts and to improve the contrast of blood elements in raw images, image preprocessing techniques should be performed. The appropriate preprocessing also helps to reduce the computational complexity in following processing phases.

Due to high resolution, accuracy and proper brightness and color balance adjustment of acquired microscopic images, there was no need to apply edge enhancing or noise reducing filtration. The proposed enhancement process is therefore based on combining standard arithmetic operations followed by the gamma correction and contrast enhancement. Using mathematical operations on individual color components allows better and more precise highlighting and differentiation of leukocytes in the image. This phase of preprocessing could be extremely useful, especially for the leukocytes with poor scanty cytoplasm. The example of the original image captured by the light microscope and the enhancement procedure is demonstrated in figure 18 and figure 19.

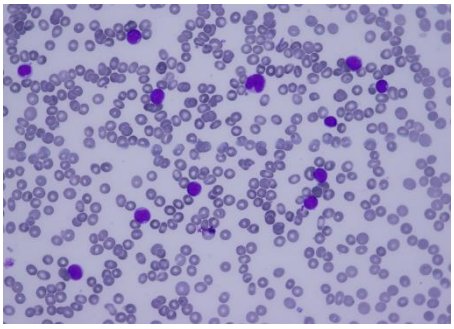

Figure 18: Original image of peripheral blood smear.

Let assume that f(x,y) is the raw digital color image, the output image g(x,y) with the enhanced WBCs is then obtained by the application of the following formula

$$f(x,y) = (R,G,B) \tag{20}$$

$$g(x,y) = [(L-1) - B] - \{[(L-1) - G] * 0.5\} \tag{21}$$

where L is the number of distinct gray levels and B, G are the blue and the green color components.

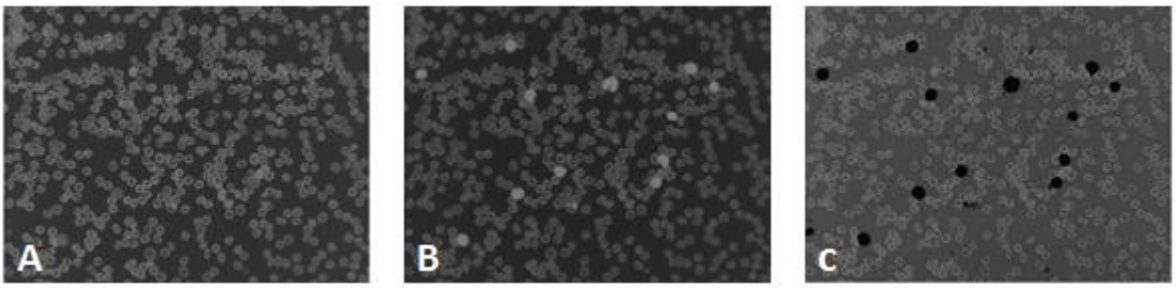

Figure 19: The proposed image enhancement: a) extracted blue plane after the application of the negative transformation, b) extracted green plane after the negative transformation, c) plane subtraction followed by the gamma correction.

5.3 Microscopic blood image segmentation

In leukemia detection and classification, leukocyte segmentation has a fundamental role. The segmentation procedure involves separating the leukocytes into individual meaningful morphological regions i.e. nucleus and cytoplasm. These segmented regions carry pivotal information about the cell structure. The accuracy of the subsequent stages in the process of classification is therefore strongly dependent on the segmentation results. The extraction of separate white blood cells from the blood smear image could be challenging due to two main reasons, the presence of a mixture of cellular blood components besides the desired leukocytes and the adjacency of leukocytes to erythrocytes and to each other. The next sections describe the proposed extraction algorithm including steps such as RBCs removal, splitting touching cells and separation of nucleus and the cytoplasm.

5.3.1 White Blood cell localization

Prior to the leukocytes extraction from the enhanced image, is the identification of the location of each white blood cell and the differentiation of these cells from the background. The main aim of individual leukocyte localization is to remove the other blood components such as erythrocytes and platelets and to separate the leukocytes or blast cells from each other. This phase comprise several image processing techniques comprising segmentation methods as well as morphological operations. The proposed automated localization algorithm consists of six fundamental steps that are demonstrated by the diagram in figure 20.

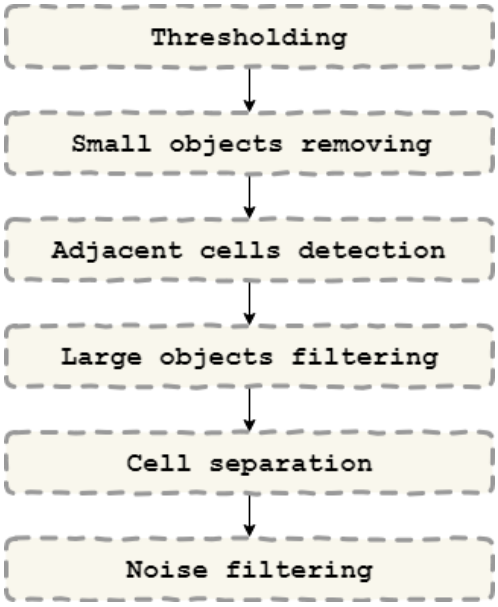

Figure 20: The proposed leukocyte localization algorithm

The fundamental operations for determining the leukocyte's location are carried out by a set of binary morphological operations. For the purpose of converting the images into binary format, a simple global threshold operation with properly selected threshold value was used. The threshold is selected in the way which will reduce a part of erythrocytes in the image while the full size of the white blood cells will be retained. Since the erythrocytes are typically shaped as biconcave disk with the inclination to overlap each other in the blood smear, the thresholding process often results in image with additional irrelevant noise.

To filter the noise and the remaining inappropriate objects such as parts of erythrocytes or larger blood film defects caused by smudging cells, three phases of filtration were proposed in the basic algorithm. Small object filtration is performed by the morphological opening operation using a disc shaped structuring element with the size of 8 pixels. This operation is achieved by erosion followed by a dilation using the same structuring element for both operations. The structural element was selected on the basis of experimental verification of several structuring elements of different shapes and sizes. The closing operations tend to preserve regions with a similar shape to the structuring element and completely remove all smaller objects. Moreover this operation allows smoothing the contours of the cells and slightly separate adjacent cells that were attached together by a thin connection. The small object filtration step is complemented with the additional limitation, which preserve only objects with the total area higher than the predefined value and thus remove the objects resistant to the closing operation.

The other filtration phases for removing large objects and blood film artifacts are based on the comparison of the particle's area and mean color derived from the histogram, with the properly chosen reference values. The results of the application of the fundamental steps in the process of localization of leukocytes are demonstrated in figure 21.

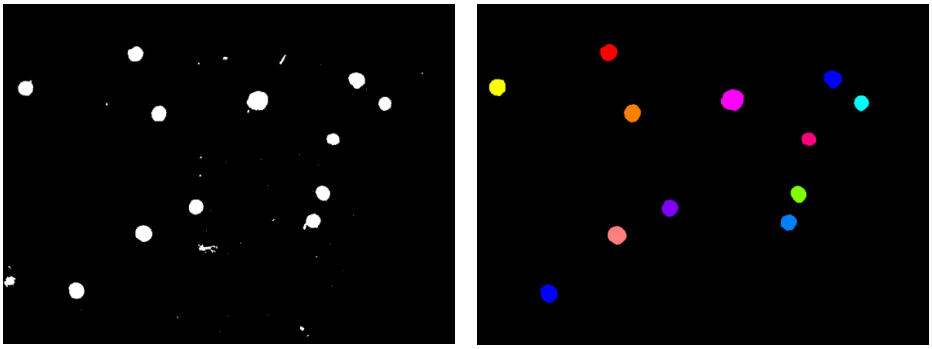

Figure 21: WBCs localization sequence: Image after thresholding (Left), image after the application of the three-phased filtration (Right).

Adjacent blasts or WBCs present in many blood smear images may cause high inaccuracy of the subsequent image processing stages. Especially shape-based features such as area and perimeter are highly dependent on the segmentation results. To achieve the best results of classification, each cell should be separated individually. To solve the problem of the detection of touching cells, the combination of morphological erosion with the total particle area computation was used. The adjacent cells were afterward separated by the application of fine edge detection technique which specifies the approximate region determining the splitting boundary (see Figure 22). To achieve the best edge detection results a 3×3 Sobel edge detection kernel for both horizontal and vertical direction was implemented.

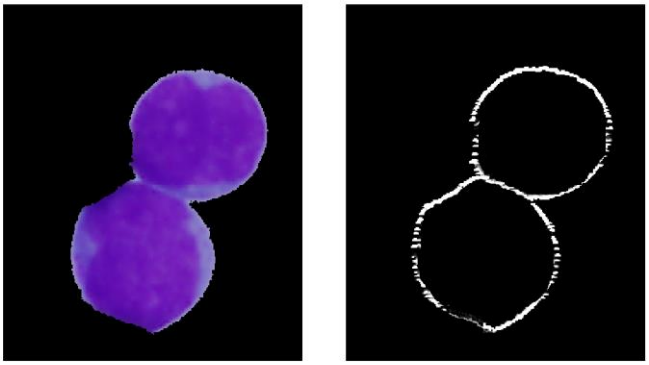

Figure 22: Application of fine edge detection technique in combination with dilatation

5.3.2 Cell regions extraction

Since the peripheral blood smear images are relatively large and comprise more leukocytes, the last part of the segmentation process consists of the extraction of individual cells and their regions into sub-images, where each sub-image contains a single leukocyte on a black background. This is a necessary step, since each WBC is evaluated for the purpose of differentiation a blast from a mature "healthy" leukocyte. Furthermore this step simplifies and increases the efficiency of the further process of the nucleus and cytoplasm separation. The coordinates of the extracted bounding box covering the cell and the estimated surrounding is given on the basis of the location of particular cells.

After obtaining the single cell sub-images, cytoplasm and nucleus area have to be extracted for the advanced analysis. The unique immature and mature chromatin patterns in nucleus vary form one cell to another, which makes the region extraction process much more challenging. The proposed extraction algorithm is presented in figure 23.

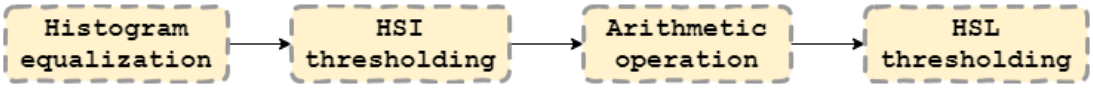

Figure 23: Nucleus extraction algorithm

This approach involves, histogram equalization to obtain more homogenous region's pixels, and application of two subsequent color thresholds extracting saturation channel from two different color spaces. Thus produce more precise determination of nucleus border. The process of particular region extraction is accomplished by the application of morphological operations defining the entire internal part of the region with the mathematical subtraction of the original image and obtained image. The results of the extraction algorithm are shown in figure 24.

Figure 24: Left to Right: Extracted blast cell, cytoplasm separation, nucleus separation

5.4 Features extraction

In general features describe the shape or texture information retrieved from the segmented pattern. The main goal of feature extraction is to obtain a set of descriptors that will be separated in various classes by classification techniques. In general, it can be defined as a function *f*, which transforms the original image *I* into a feature vector *x*, where *d* is the number of features.

$$f : I \rightarrow x = (x_1, x_2, \dots, x_d) \tag{22}$$

This technique therefore reduces the data dimensionality and redundancy, which allows preserving only the variables containing the most discriminatory information. [44]

For the problem of acute leukemia diagnosis and classification features extraction plays vital role due to the specific characteristics of the nucleus and the cytoplasm of leukemic cells. It is used to

extract the features in a similar way to those visually detected by hematology specialists, who accurately identify the blast cells. For this purpose sixteen features were extracted from each cell in the image. This included 9 morphological features and 7 statistical or texture features. All features selected in this thesis for the purpose of differentiation of leukemic cells from the normal cells, are chosen on the basis of the conducted research study. The detailed overview of selected features is listed in the following subchapters.

5.4.1 Geometrical features

Medical image processing techniques, especially blood cell diagnostic systems has been largely based on the morphological features of objects. Blast cells presented in acute types of leukemia are characterized by unique shape properties comprising area, perimeter, circular bounding, axis length etc. The following selected shape features attempt to quantify the morphological appearance of blast cells in ways that agree with the perception of domain experts.

- **Cell area –** the total number of pixels within the interior of the cell.
- **Cytoplasm area –** the total number of pixels within the interior of the cytoplasm of the cell.
- **N/C ratio** – the ratio of the size of the nucleus to the size of the cytoplasm of the cell. In clinical diagnosis, this feature is considered as a major characteristic of the maturity of a cell.
- **Nucleus perimeter** – the total number of pixels representing the nucleus boundary.
- **Nucleus compactness** – quantitative representation of the degree to which a shape is compact. The measure is given by the relation

$$Compactness = \frac{perimeter^2}{area} \tag{23}$$

- **Nucleus form factor** – measure of the shape irregularities. The measure is a dimensionless parameter defined as

$$Form\ factor = \frac{4 * \pi * area}{perimeter^2} \tag{24}$$

- **Nucleus eccentricity** – measure of how much a shape deviates from being circular. The eccentricity is calculated as a ratio of the length and the width of the minimal bounding rectangle of the ROI.

$$Eccentricity = \frac{bounding\ rectangle\ lenght}{bounding\ rectangle\ width} \tag{25}$$

- **Nucleus elongation** – quantitative measure of the abnormal bulging. It is defined as the ratio of the minimum to the maximum distance from the center of gravity to boundary.

- **Nucleus solidity** –describes the extent to which the shape is convex or concave and is defined as the ratio of the area and convex hull area [44] [45]

5.4.2 Texture features

Another important features used for the blast cell detection are based on the changes in the chromatin structure of nucleus and cytoplasmic changes. The diverse distribution of chromatin reflects the formation of DNA in leukocytes. For that reason the chromatin texture is considered as the pivotal descriptor during the malignant cells classification. In order to capture the essential information about the structural arrangement of surface, two types of textural features are used. The first order statistical features based on the histogram of an image and second order statistical features derived from the gray level co-occurrence matrix (GLCM).

The first order histogram based features are extracted from the histogram of a grayscale image. Unlike the second order statistical features, these features estimate properties of individual pixels without taking into account the spatial interaction and correlation between the neighboring pixels. The most common features include moments such as mean, variance, skewness and kurtosis. For the malignant cell classification only the first moment of inertia is calculated from the nucleus and the cytoplasm of the cell. This gives the average gray level of each region. The first moment is given by the formula

$$m_1 = \sum_{i=0}^{L-1} z_i P(z_i) \tag{26}$$

where z is a random variable denoting the gray levels of image region, L is the number of gray levels and $P(z_i)$ is the probability density function of the pixel defined by the equation (27).

$$\mathrm{P(z)} = \frac{number\ of\ pixels\ with\ gray\ level\ z}{total\ number\ of\ pixels\ in\ the\ image\ region} \tag{27}$$

Since the texture descriptors based solely on the histogram can´t provide the information about the relations among pixels or a group of pixels, these features cannot help to distinguish between the completely different images producing the same gray level histogram. To bring the position information of the pixels into the texture analysis process, second order statistic methods were introduced by Haralick et al. This type of feature extraction is based on the matrix of relative frequencies which describes the frequency of appearance of two pixels in the image. The gray level co-occurrence matrix, also called as gray level dependency matrix is therefore defined as a two dimensional gray level histogram for a pair of pixels, that are separated by a fixed distance along a specific direction (usually horizontal, vertical, diagonal and anti-diagonal). Figure 25 illustrates the process of formation of the GLCM for the horizontal direction with a step of 1. [46]

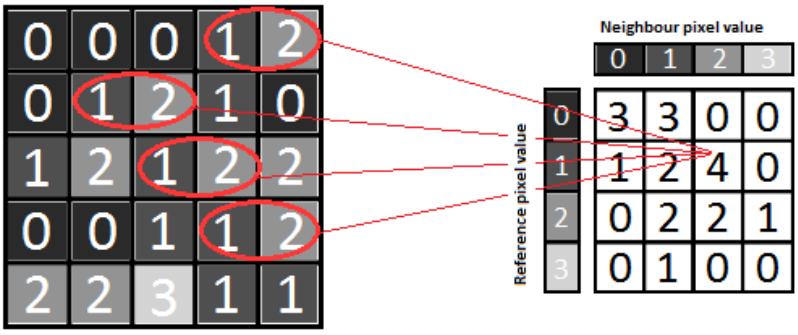

Figure 25: An example of GLCM computation for a matrix 4x4 of four gray levels represented by numerical values from 0 to 3.

The most well-known and widely used texture descriptors were proposed by Haralick. These fourteen features are generated by averaging the values obtained from separate co-occurrence matrices calculated for each main direction (particularly for 0, 45, 90, and 135 degree clockwise). In practical use some of these features may be highly correlated, which means that they are not valuable for the classification algorithm. For this reason this thesis concern only five Harralick textural features performed on the whole cell and the segmented nucleus.

The detailed description of chosen features is given by the following equations, where *P(i, j)* is the element of the normalized co-occurrence matrix at the coordinates *i* and *j*, N_g denotes the number of distinct grey-levels and μ_x, μ_y and σ_x, σ_y are the means and standard deviations of the normalized GLCM.

- **Nucleus energy** – statistical feature also denoted as angular second moment. It measures the local textural uniformity of gray levels. The energy increases with the homogeneity of the image and is defined thus

$$Energy = \sum_{i,j=0}^{N_g-1} \left(P_{i,j}\right)^2 \tag{28}$$

- **Cell contrast** – measures the amount of local variations in the image. It is measured between the reference pixel and its neighbor. Generally, high contrast values reflect large intensity differences in the co-occurrence matrix. The relation is given by the following formula

$$Contrast = \sum_{n=0}^{N_g-1} n^2 \left\{ \sum_{i=1}^{N_g-1} \sum_{j=1}^{N_g-1} P(i,j) \right\}, |i-j| = n \tag{29}$$

- **Nucleus correlation** – measure of the linear dependency of gray tone values in the GLCM. It specifies the degree of correlation of a pixel to its neighbor and is defined by the following equation

$$Correlation = \frac{\sum_i \sum_j (i,j)P(i,j) - \mu_x \mu_y}{\sigma_x \sigma_y} \quad (30)$$

- **Cell dissimilarity** – also called as difference average. It measures the mean of the gray level difference distribution of the region and is defined thus

$$Dissimilarity = \sum_{i=0}^{N_g-1} \sum_{j=0}^{N_g-1} |i-j|P(i,j) \quad (31)$$

- **Cell entropy** – is a measure of the complexity or the randomness of a texture. Homogeneous images are characterized by lower entropy value while the heterogeneous region results in higher entropy. The entropy can be calculated using the formula [46] [47]

$$Entropy = -\sum_{i=0} \sum_{j=0} P(i,j) log P(i,j) \quad (31)$$

5.4.3 Statistical evaluation of extracted features

All textural and geometrical features are validated by using statistical hypothesis testing method. The validation was realized for the purpose of determining whether the samples representing the leukemic and normal cells come from the same population or whether the distribution of the independent variables is the same for both groups. Since the given data do not come from the normal distribution (determined by Shapiro-Wilk normality test), the median and median absolute deviation[8] (MAD) was selected as the appropriate measure to describe the observations in the given dataset. In general, features are considered to be separable in case of sufficiently different median and low values of MAD.

The statistically significant difference between the two populations is evaluated by the Man-Whitney U test. The general example of the null and alternative hypothesis statement used for the purpose of statistical determination of the differences between features retrieved from leukemic and normal cells is given below.

H_0: The distributions of the two groups are equal
H_A: The distributions of the two groups are not equal
Significant level: 0.05

The null hypothesis can be rejected in case that p-value is less than the selected significance level. The p-values, respectively the probabilities that the distributions or the changes of median values of the two observed groups are not significantly different are listed in table 5.

[8] Robust statistical measure of how spread out the dataset is.

Table 5: Quantitative validation of selected features

Features	Normal cell		Leukemic cell		U test p-value
	Median	MAD	Median	MAD	
Cytoplasm area	11985.00	4894.53	4022.00	1799.24	<< 0.001
Cell area	20011.00	6031.12	16255.00	2830.51	<< 0.001
N/C ratio	0.75	0.21	3.15	1.15	<< 0.001
Nucleus perimeter	521.00	112.64	412.00	58.51	<< 0.001
Nucleus compactness	30.71	14.14	13.13	2.47	<< 0.001
Nucleus form factor	0.41	0.19	0.96	0.18	<< 0.001
Nucleus elongation	6.97	7.12	1.62	0.31	<< 0.001
Nucleus eccentricity	0.49	0.23	0.42	0.18	0.007
Nucleus solidity	0.84	0.09	0.96	0.02	<< 0.001
Nucleus energy	0.74	0.05	0.61	0.04	<< 0.001
Cell contrast	1.85	0.16	1.53	0.13	<< 0.001
Cell entropy	7.37	1.42	5.15	1.20	<< 0.001
Nucleus correlation	0.82	0.08	0.89	0.05	<< 0.001
Cell dissimilarity	0.56	0.08	0.40	0.07	<< 0.001
Cytoplasm mean color	2.34	0.92	0.73	0.34	<< 0.001
Nucleus mean color	0.37	0.20	0.57	0.22	<< 0.001

According to Table 5, the null hypothesis at the 5% level of significance is rejected in all cases. Fifteen features are strongly unique with a great difference between the normal cells and blasts. Although the eccentricity of the nucleus results with much more lower p-value, this feature still remains statistically significant and plays an important role in the further classification.

5.4.4 Data normalization

Often the dataset contains features that highly vary in magnitudes, units and range. Since most of the classification algorithms are based on the Euclidian distance between two data points, different ranges could cause complete domination of one factor over another. This usually results in less accurate or incorrect classification. To suppress the effect of non-uniform features, it is necessary to perform the data normalization for each attribute of a feature vector before the classification process. It allows not merely more uniform influence for all weights but also faster convergence on learning.

The simplest approach to standardize the range of various independent variables is to rescale the range. The min-max algorithm scales a variable in training samples in the range of values lying within a predetermined range of < 0, 1 >. This step is realized by using the following formula

$$X_{norm} = \frac{X - X_{min}}{X_{max} - X_{min}} \tag{32}$$

where X is the original value from feature vector, X_{norm} is the scaled value and X_{min} and X_{max} are the minimum and the maximum of a given vector. [48]

5.5 Blood cell classification

The main goal of the classification is to distinguish between the normal and cancerous cells. The classification step classifies the input data of unknown cells to one of the predefined classes on the basis of the features extracted in the previous stage. This is carried out by supervised classifications which use one dataset, containing leukemic as well as normal cells. In the process of the final classification, the set of measured data is divided into two sections, the training and testing data set. The training set consists of 144 segmented cells, where the ratio of blasts and normal leukocytes is uniform. These data are primarily used to construct a classification model based on the given data before the unknown data classification, or to update weights of the particular features during the training process. The remaining data are used for the testing of the performance of individual classifiers. To preserve the appropriate size of the dataset, the process of validation and finding the optimal classifier parameters is realized on the whole range of samples.

The performance of extracted features may differ depending on the chosen classifiers. For the purpose of white blood cells evaluation, the two most popular classifiers in medicine were used. Thus include support vector machine classifier and artificial neural networks. A detailed summarization of the selected classification methods is provided in next subsections.

5.5.1 Support vector machine

Support vector machine, shortened SVM, is one of the most popular supervised classification algorithms with the ability to handle noisy and high dimensional data. In simple term the SVM classification tries to find an optimal line or a hyperplane separating the objects having different class memberships. Hyperplane could be defined as a flat n-1 dimensional subset of n-dimensional space, which divides this space into isolated parts. Depending on the given labeled training data, the SVM constructs the hyperplane or a set of hyperplanes for a high-dimensional space, which is able to categorize new unknown samples into predefined classes. The samples or the data points that are nearest to the boundary are called as support vectors.

Suppose to have a training dataset $[(x_1, y_1)\dots (x_n, y_n)]$, where x_i and y_i are the feature vectors representing the given observations and their labels. Let define the vector y as follows

$$y_i = \begin{cases} 1 & if\ x_i \in (class\ 1) \\ -1 & if\ x_i \in (class\ 2) \end{cases} \tag{33}$$

The SVM method then tries to separate the given samples (labeled with the value 1 and -1) by a hyperplane in such a way that the separation between the two classes, denoted as margin, is as wide as possible. The margin is defined as the shortest distance between the particular classes and is measured along a line which is perpendicular to the constructed hyperplane. This type of the

hyperplane is also known as maximum-margin hyperplane. Figure 26 illustrates the optimal separating hyperplane for a data in a two-dimensional space. [51]

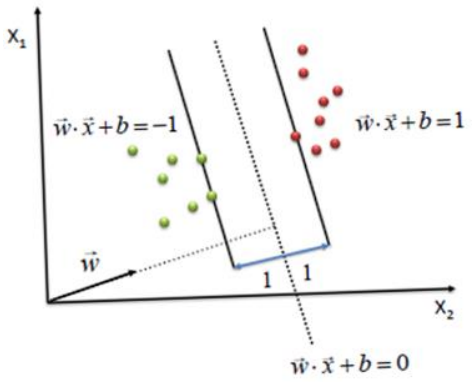

Figure 26: Definition of the optimal hyperplane. [11]

Let the green circles symbolize the data belonging to the first class and the red colored circles symbolize the second class data. The separation of two classes could be usually performed by several hyper-planes. Regarding the maximum-margin hyperplane concept, such a line or hyperplane parameters (w, b) must be found, that the distance between the hyperplane and the observations is maximized. To calculate the distance between the particular instances and the hyperplane, the Euclidean distance is used. The general formula of the hyperplane is given by the following equation

$$w^T x + b = 0 \tag{34}$$

where x is an instance in a n-dimensional space and w and b are the hyperplane coefficients, specifically the vector of weights perpendicular to the hyperplane and the bias determining the position of the hyperplane with respect to the origin. In a problem of a binary classification, the decision function is therefore denoted as

$$y_i = \begin{cases} 1 & if\ w^T x + b \geq 0 \\ -1 & if\ w^T x + b < 0 \end{cases} \tag{35}$$

In a binary classification the hyperplane coefficients can be obtained by using the Lagrange multiplier method to minimize the constrained optimization problem demonstrated by equation (36). The Lagrange multiplier finds the maxima and minima of a function with subject to certain constraint by defining a function, which takes its partial derivative and equalize it to zero. [52] [53]

$$\begin{aligned} &\min_{w,b}\ \frac{1}{2} w^T w \\ &subject\ to \quad y_i(wx_i + b) \geq 1, i = 0, \dots, l \end{aligned} \tag{36}$$

In real world, most of the classifications deal with the data that cannot be linearly separated. Therefore in most cases non-linear hyperplane is needed. This could be done by mapping each feature vector in the original dimension into a higher dimensional feature space through some non-linear mapping function. This is denoted as a Kernel trick. Although mapping points into higher dimensions increase the complexity and computational difficulty it still remains as a necessary step for the correct separation. The biggest advantage of using Kernel is that it is not necessary to calculate the transformed vectors explicitly to find the maximum margin hyperplane. Since the kernel functions allows operating in the sub-regional space where observations gain linear structure, using Kernel function can eliminate the explicit calculation of the individual transformed vectors. Figure 27 shows the transformation of the two-dimensional input space to feature space. [51] [53]

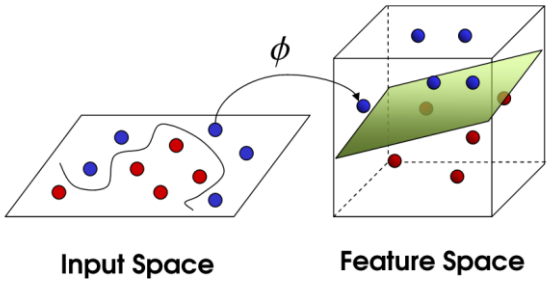

Figure 27: Kernel trick: Transformation into a three-dimensional feature space. [12]

For the practical implementation of the SVM, the soft margin classification method was selected. This method is able to deal with the non-separable data by allowing misclassifications during the data training. The decision boundary obtained in this manner is called as soft margin. This may produce larger margin and more generalizable classification model when the new dataset is applied. Thus allows higher accuracy of the classification of unknown samples in comparison with a decision boundary with no training errors and smaller margin.

The required property of the large margin is achieved by introducing slack variables ξ_i, which represent the deviation of the instances from the margin. In simple term the slack variable corresponds to errors and is equal to zero in case that the instance is located on the correct side of the hyperplane. On the other hand, if observations appear on the wrong side of the hyperplane, the slack variable is greater than zero. In order to regulate the balance between the number of training errors and the margin value, the soft margin method uses cost parameter. Generally, this parameter specifies the penalty for misclassifications. High values of the cost parameters prohibit training errors and may tend to over fit the training data, while lower cost values produce softer margin with a higher tolerance for the training errors. In accordance with the introduced parameters the optimization problem can be reformulated as

$$\min_{w,b} \ \frac{1}{2} w^T w + C \sum_{y=1}^{l} \xi i \qquad (37)$$

$$subject\ to \quad y_i(w^T k(x_i) + b) \geq 1 - \xi i,\ \xi i \geq 0,\ i = 0, \dots, l$$

where w is the normal vector of the hyperplane to origin, ξ_i is the slack variable which soften the borders by allowing some instances to fall off the margin under certain penalization and C is the cost parameter. [53] [54]

5.5.1.1 SVM model selection

For the selection of an appropriate SVM classification model, various kernels were experimentally used. This included the most common linear kernel and a set of non-linear kernels comprising Polynomial, Gaussian and Radial basis function kernel. The accuracy of the chosen kernels on the given samples is demonstrated in table 6. The following evaluations are performed on the set of 123 immature and 118 mature white blood cells from 31 blood smear images. This part of the verification uses the same dataset for the SVM model training as well as for the classification.

Table 6: Experimental verification of the classification efficiency of different SVM classification models on a trained data.

Kernel function	Leukemic cells detection [%]	Normal cells detection [%]	Total accuracy [%]
Linear	88.62	88.98	88.80
Polynomial	100.00	100.00	100.00
Gaussian	98.37	98.31	98.34
RBS	99.19	98.31	98.75

For a better evaluation and prediction of the behavior of classification models, the cross validation technique was performed. This statistical model, also known as out of sample testing, estimates the accuracy of the performance of predictive model on the independent unknown data. To verify the given dataset k-fold cross validation methodology was selected. This method is based on a single parameter k, which refers to the number of groups to which the input dataset is divided. For the purpose of this study the 10-fold cross validation technique has been used. This value has been found through experimentation that produces the best out-of-sample estimates with low bias and modest variance.

The initial dataset comprising 241 samples with 16 features per each sample was randomly partitioned into ten folds of equal size. During the cross-validation process, one of the folds is retained as the validation data for testing and the rest of folds are used as training data. This cycle is repeated for 10 times whereas each fold is used once as a validation testing data. The results of the individual iterations are afterward averaged or computed by other alternative methodologies to obtain a single estimation. The final accuracy of the tested classification model is computed by the following formula and the results reflecting the impact of using different kernels are demonstrated in table 7.

$$Accuracy = 100\ \frac{Number\ of\ samples\ classified\ correctly}{Total\ number\ of\ samples} \tag{38}$$

Table 7: Cross validation accuracy of different classification models.

Kernel function	Accuracy [%]
Linear	88.38
Polynomial	98.34
Gaussian	95.02
RBS	97.51

As experiments conducted, the optimal kernel function for the SVM classification of the white blood cells is the polynomial kernel. In comparison with the other classification models, the polynomial kernel achieved the best results in both experiments with the cross validation accuracy of 98.34 %.

5.5.2 Artificial neural networks

Artificial Neural Network (ANN) is a classification and machine learning system which attempts to process the information in such a way the biological neural network does. Biological neural networks consist of an enormous amount of organized nerve cells, called neurons, which interact with each other in parallel. The signal from each neuron is transmitted through synapses, which are electrochemical joints between the branches receiving the signals, called dendrites, and terminal branches (axons). Whenever the received signals become strong enough and exceed a certain threshold, the neuron is activated and emits the signal through the axon. In addition, the biological neural networks during the learning continuously change and update themselves, especially the connections between particular neurons. This allows remodeling the architecture of the inner neural structure with strengthening or weakening the particular connections depending on the gained experience.

Application of this functionality in machine learning may solve various problems which are too complex to be noticed or performed by either humans or other computer techniques. By training, a neural network can become an "expert" in the field of the information it has been given to analyze. Usually, the standard applications of ANN cover pattern recognition, image or signal processing, forecasting or object classification.

Since the biological neurons are very complex, the model of artificial neuron is highly abstracted and simplified. A prototypical example of the elementary unit of the artificial neural network is shown in Figure 28.

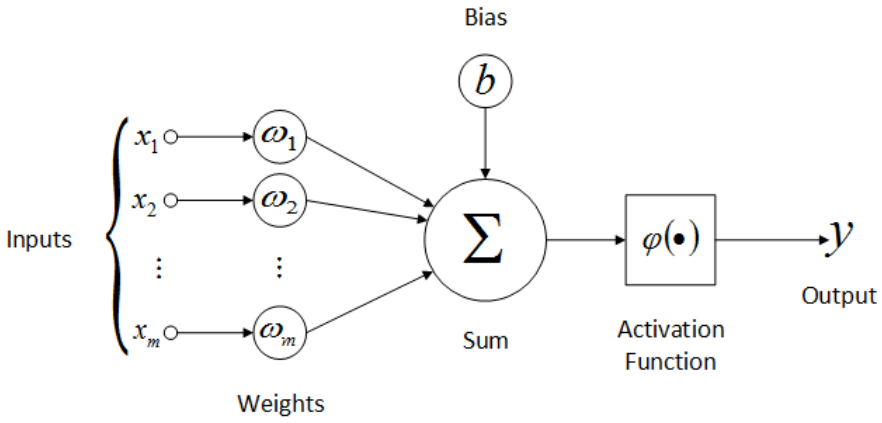

Figure 28: The mathematical model of artificial neuron. [13]

Each input in a neuron is separately weighted by parameter *w* which can be modified during the learning process. The single number of weights represents the particular synapses and determines the prominence of the respective inputs to the output. Higher weights produce stronger inputs and the prominence of the signals linearly increases with the multiplication value. In certain cases the weight might be also negative and therefore inhibit the input signal. Prior to the evaluation of the neuron's output, each weighted input signal is mathematically transformed to obtain a single value. This is usually achieved by applying the summation operator in combination with the bias parameter which controls the influence of neuron as a whole and so helps the model to fit better on the given data. The biases and weights are then gradually shifted towards a desired output with each learning cycle. The final activation of each neuron is usually ensured by a nonlinear transformation of its input. This is performed by the activation or also called transfer function, which decide whether the receiving information is relevant or should it be ignored. [55]

Let M be the total number of input signals x_i with their corresponding weights w_i. The φ denotes the defined activation function and b is the bias. The output of each neuron is then calculated by the following equation

$$y_i = \varphi\left(\sum_{j-0}^{M} w_{ij}x_j + b\right) \tag{38}$$

Over the past few years several different activation functions were proposed to determine the boundary of the neuron's output. The earlier artificial neurons denoted as perceptrons were based on the simple binary threshold function, which can take on only two values. This function is also referred to as step or Heaviside function. The mathematical formulation of the step activation function is given below

$$\delta(x) = \begin{cases} 0 & if\ 0 > Threshold \\ 1 & if\ 0 \leq Threshold \end{cases} \tag{39}$$

The output of the neuron is determined by whether the weighted sum of the input signals is less than or greater than some threshold value. In case that the input is above a threshold, the value of the function changes, otherwise it remains constant. This implies that the step function is non-differentiable at the threshold and hence it fails in the weight updating task. Due to this fact, the backward propagation of errors during learning is impossible. To overcome, this problem other activation functions, which replace the step function were introduced. One of the most widely used transfer functions is the sigmoid. The mathematical form of this function is defined as

$$\varphi(x) = \frac{1}{1 + e^{-x}} \tag{40}$$

This non-linear function maps real-valued output in a range between 0 and 1.The advantage of the sigmoid neuron is the high steepness in the middle area, which brings the *y* (output) values to the extremes of the curve and thereby enables clear predictions. Towards the either end of the sigmoid function, the output values tend to respond noticeably less to changes, which gives rise to the biggest undesirable problem of "vanishing gradients". This means that the extremely small values cannot make significant changes to the output and the learning of the network is slackened. The graphical representation of the sigmoid and step function is illustrated in Figure 29. [55] [56]

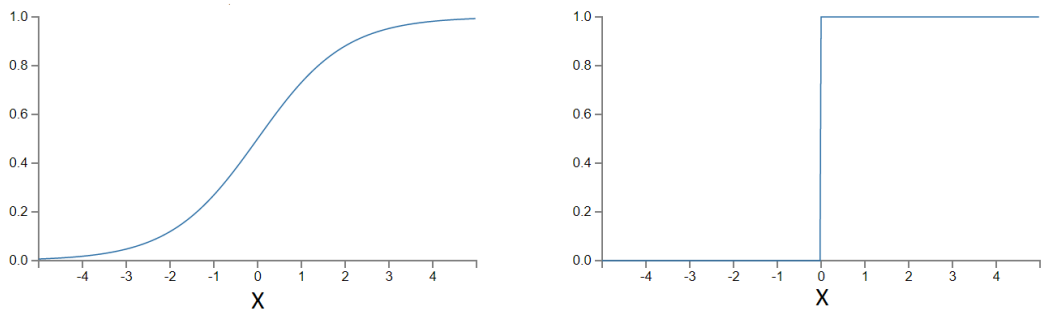

Figure 29: Comparison of the activation functions: Sigmoid function (left), Step function (right). [14]

5.5.2.1 Neural network topology

The architecture of ANN is often organized into distinct layers of a certain number of neurons which take in the input signals and provide the output. The most common type of the neural network is the fully-connected network, where particular neurons between two adjacent layers are fully pairwise connected, while neurons within the layers have no connections. Usually neural networks consist of three basic sections, the input layer, the output layer and a group of several hidden layers. The typical structure of the simple neural network is shown in Figure 30.

The input layer contains a set of input neurons which provide information from the external environment to the network. These neurons just transfer the inputs to the hidden layers and do not perform any computation. Neurons in a middle layer are neither inputs nor outputs (hence the terminology hidden). These layers are thought to be the basis of the neural network since they process

the inputs obtained by previous layers and send the final information to the output layer. The number of hidden layers as well as the number of neurons in any given layer may differ depending on the complexity of the problem. Nevertheless it has to be noticed that with the increasing complexity, increases the chance of overfitting, which means that the performance of the classification on the testing set is much lower than the performance on the training data. Unlike hidden layers of the ANN, the neurons in the output layer often do not have a non-linear activation function and rather uses linear identity function. This is by the reason that the last layer results represent the classification scores, or in other words, the probabilities of the memberships to particular classes. The number of neurons in the last layer, therefore, should be directly related to the proposed problem. [57]

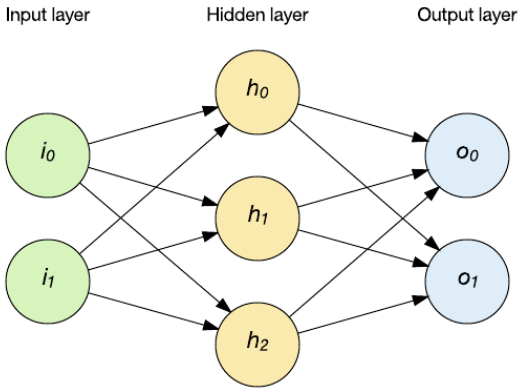

Figure 30: Fully-connected three-layered neural network.

There are different concepts to set up the hidden layers, which will generate various results. The most popular type of hidden layers used in the field of signal and image processing are given below.

- Fully-connected layer – each neuron has weighted connection to every neuron in the previous layer

- Convolutional layer – forms the core building block of a convolutional neural network and its main objective is the extraction of high-level features by performing the convolution operation (see Chapter 4.2.2) across the whole image

- Pooling layer – reduce the dimensionality of the convolved features and helps to extract only the dominant features

- Loss layer – specifies the penalization for the incorrect predictions

- Dropout layer – regularization technique used to prevent overfitting by deactivation of half of neurons on a particular layer [58]

5.5.2.2 Backpropagation

During the process of learning the neural network calculate the total error at the output and through the backpropagation algorithm, which computes the gradients in each layer, propagate them back to the network. The gradients in each layer are computed by finding the derivatives of loss function with respect to any weight in the network. This is simplified by applying the chain rule, which helps to identify how much each weight contributes to the overall error. All weights and biases in the network are afterwards adjusted by using a gradient descent optimization method that minimizes the loss function.

Usually, the loss function is calculated as the difference between the actual value and the desired output value. There are several different approaches to compute the output error, or alternatively the loss function. The simplest method is the mean squared error (MSE) that measures the differences of the predictions and actual values. Since the MSE is characterized by slow divergence when using sigmoid activation function, it is often replaced by cross entropy that measures the divergence between two probability distributions. Both mentioned loss functions are quantified by the following equations

$$MSE = \frac{1}{n}\sum_{i=1}^{n}(y_A^{(i)} - y_P^{(i)})^2 \tag{41}$$

$$E = -\frac{1}{n}\sum_{i=1}^{n}\left[y_A^{(i)} log\left(y_P^{(i)}\right) + (1 - y_A^{(i)}) log\left(1 - y_P^{(i)}\right)\right] \tag{42}$$

where n is the number of training examples and $y_A^{(i)}$ and $y_P^{(i)}$ is the actual and the predicted value at the output of the neural network. [61]

To demonstrate the backpropagation algorithm applied in this thesis, figure 31 illustrates a two-layered network, where the loss function for each neuron in the output layer is calculated by the Equation (41).

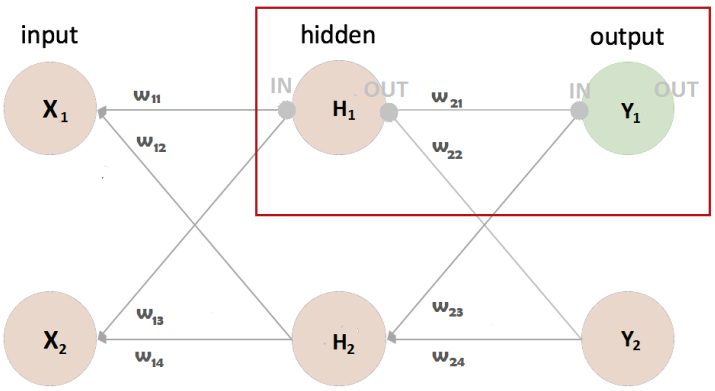

Figure 31: Structure of a two-layered ANN, with the corresponding variables

Each neuron is represented by a function of the previous layer connected to this neuron. Therefore by updating the value of the w_{11}, both hidden layer neurons and the output neurons, would change. Because of this notion of functional dependencies, the output can be mathematically formulated as an extensive compound function

$$Y_1 = \varphi[\varphi(X_1 w_{11} + X_2 w_{13}) w_{21} + \varphi(X_1 w_{12} + X_2 w_{14}) w_{23}] \tag{43}$$

where Y_1 and X_1 are the output and the input layer neurons of the neural network, $w_{11} \ldots w_{14}$ are the particular weights of the neuron inputs and φ is the activation function of the hidden layer neuron and output neuron (refer to Eq. 40, page 56).

In the backward pass to compute how the loss function changes with changing weight, the derivative of the error function has to be computed for each weight. To find the derivative of such a compound function with respect to some arbitrary weight the chain rule method is iteratively applied. In simple term this composite function rule differentiates the 'outer' function, and then multiplies it by the derivative of the 'inner' function. The following formula demonstrates a simple example of the calculation of the loss function at the output with respect to w_{21}.

$$\frac{\partial E}{\partial w_{21}} = \frac{\partial E}{\partial Y_{1\_OUT}} \frac{\partial Y_{1\_OUT}}{\partial Y_{1\_IN}} \frac{\partial Y_{1\_IN}}{\partial w_{21}} \tag{44}$$

where Y_{i_OUT} and Y_{i_IN} are the output and the input of the neuron in the i-th neuron located in either output or hidden layer. Each of these derivatives can be simplified by replacing these abstract notations with the activation and error functions, such that the loss function results would represent a numerical value. By replacing the partial derivatives in the expression above, the following formulas can be obtained. The first partial derivative reflects the change in error in the output layer and is derived as the partial derivation of the loss function defined by the MSE equation.

$$\frac{\partial E}{\partial Y_{1\_OUT}} = \frac{\partial \left[\frac{1}{2} (y_A^{(i)} - y_P^{(i)})^2 \right]}{\partial y_A^{(i)}} = y_A^{(i)} - y_P^{(i)} \tag{45}$$

Since the relation between the input and the output of a certain neuron is defined by the sigmoid activation function, to calculate the change of the neuron's output with respect to its input, the partial derivative of this function is taken. The second derivative of the chain is then defined as follows

$$\frac{\partial Y_{OUT}}{\partial Y_{IN}} = y_A^{(i)} (1 - y_A^{(i)}) \tag{46}$$

The last term of the equation encompasses the input of the hidden layer which proceeds through a transfer function. Considering the forward propagation, where the linear combination of weighted outputs of the hidden layer passes into the sigmoid function, the partial derivative of the neuron's input with respect to the weight w_{21} can be then given by the formula (47). Performing the

partial differentiation with respect to a certain weight, all remaining weights in the neuron's input are treated as constants and hence the derivatives are taken as zeros.

.

$$\frac{\partial Y_{1\_IN}}{\partial w_{21}} = \frac{\partial (H_{1_{OUT}} w_{21} + H_{2_{OUT}} w_{23})}{\partial w_{21}} = H_{1\_OUT} \tag{47}$$

To update the specific weight, gradient descent optimization method is applied. The canonical formula for the ordinary gradient descent for updating w_{21} is defined by the equation below, where α is the learning rate denoting the speed of the parameter updating and $\frac{\partial E}{\partial w_2}$ is the computed partial derivative of the loss function with respect to the particular weight.

$$w_{21} = prior\_w_{21} - \alpha \frac{\partial E}{\partial w_{21}} \tag{48}$$

This process is performed on each weight in each layer for all the samples in the training data until there is a convergence in the loss function. [59] [60]

5.5.2.3 The proposed model of neural network

Since the topology of the neural network directly influences the classification capability and the computational complexity, it is essential to propose appropriate network architecture. This task consists of a few steps including activation function selection and determination of the number of hidden layers with the number of neurons in each layer. The amount of neural units in the input and output layers depends on the given model's inputs and desired outputs. The input layer of the proposed ANN consist of sixteen neurons (one neuron per each extracted feature), while the output layer has two neurons, representing the leukemic and the normal class.

In spite of the fact that there are no specific guidelines how to determine and select the optimum number of both, hidden layers and neurons, this parameter is in practice often selected through a trial and error process. To determine the optimal architecture of the neural network, different neural networks of various numbers of neurons and hidden layers were experimentally tried. The performance of the individual models is summarized in Table 8. Depending on the type of the given data, all neurons in all layers are based on a sigmoid activation function. To train the neural networks in this thesis, the back-propagation algorithm was used. For this purpose 241 individual WBCs were given as the primary dataset. This dataset was divided to the training and validation set in a general convention ratio 80:20.

To avoid the overfitting and concentration of the neural network to one domain, the learning process was based on the learning of randomly selected samples. This selection method can be described by the constant distribution function, and hence for the training process two different numbers of learning iterations were chosen. The first sequence of neural network training was set to 10 000 iterations. This value at the constant distribution function and a total of 200 learning samples resulted in an average value of 50 for one sample learning. For the improvement of the subsequent

learning cycles the number of iterations was enlarged 10 times. Each learning cycle uses identical learning rates, which ensure the uniform influence of all training samples

Due to the random selection of the particular neural network coefficients before the learning process, the whole learning is burdened with an initialization error. This effect could cause that the result of the neural network won't be able to find an optimization global minimum but just a local minimum, which reduces the accuracy of the evaluation itself. To reduce this uncertainty, the learning process of each proposed neural network was realized more than once with the nominal value of 10 iterations.

Table 8: Experimental evaluation of the accuracy of different structures of ANN

Number of neurons in hidden layers				Accuracy [%] 50 LI	Accuracy [%] 500 LI
1st layer	2nd layer	3rd layer	4th layer		
50	-	-	-	92.38	99.58
90	-	-	-	92.14	99.53
100	-	-	-	92.67	99.53
500	-	-	-	90.43	99.32
50	30	-	-	93.14	99.90
70	50	-	-	93.89	99.69
100	100	-	-	91.28	99.69
400	200	-	-	93.56	99.91
200	400	-	-	91.46	98.77
100	100	100	-	91.87	98.52
200	100	200	-	90.91	99.80
500	300	100	-	94.44	99.91
500	400	300	-	92.34	99.49
100	100	100	100	91.17	99.44
700	500	300	100	95.49	99.91

* Learning iterations

The particular topologies of ANN were selected in such a way, which will fully cover the whole spectrum of undesirable phenomena that may occur in these networks. The examples of most common issues in neural network application are listed below.

- *Shallow/Deep ANN* – where every neural network with a too small number of layers may not obtain every required input value correctly and in the contrary too deep networks may lose crucial information between single layers.

- *Ascending/Descending ANN* – neural networks with the first layer containing smaller amount of neurons followed by layers with higher number can introduce certain entropy into the system. That is manifested by a higher amount of duplicate information, which is due to

different errors transmitted in the form of different values. In case of the opposite problem, the information flowing from larger layers to smaller ones can be lost in a way that the desired information is not transmitted in a sufficient form to any of the subsequent neurons.

The experimental verification of proposed neural network topologies revealed that the accuracy of the neural networks with lower learning iterations increased with the number of hidden layers, as well as with the larger amount of neurons in particular layers. The only exception was the most complex neural network architecture with four hidden layers and high number of neurons (700 neurons in the first layer), which reached the highest accuracy of 95.49 %. On the other hand, neural networks with 500 learning iterations and increasing number of hidden layers as well as number of neurons demonstrated significantly greater precision and ability to classify the given data correctly. The highest accuracy of 99.91 % was reached by the ANN models with a sufficiently large difference in number of neurons between the particular hidden layers, specifically 200 neurons.

6 Experimental evaluation of proposed methods

The principal aim of the experiments is to evaluate the performance of the selected classifiers trained with the given dataset and compare the proposed approaches to other found in literature, regarding the accuracy rate. Since there could be many differences among the images according the resolution, magnification and lightening during the acquisition, all images were captured by the same camera with the same lightening conditions. The whole process of verification of individual cells extracted from 31 peripheral blood smear images has been established based on the further consultation with a domain expert.

In this analysis 241extracted sub images of 118 healthy leukocytes and 123 blast cells are used for the system evaluation. To obtain more reliable classification results, forty percent of the data was assigned for the training subset used to build the prediction model while sixty percent of the data was used to test the model. The training and testing datasets is built in the way that both sets contain similar ratios of healthy and leukemic cells, which ensures proportional distribution of particular classes. To verify the proper division of the data between the training and testing set, statistical parameters are evaluated for each subset. It has to be noticed that the fundamental statistical parameters listed in Table 9 got to be close to each other in both subsets.

Table 9: Statistical properties of training and testing data set

Statistical parameter	Training set	Testing set
Number of samples	*97*	*144*
Maximum value	33 935	42 547
Minimum Value	0	0
Mean	1 842	1 820
Standard deviation	5 447	5 420

6.1 Performance analysis

In general, performance of the classification algorithm is evaluated using a matrix known as the confusion matrix. The confusion matrix contains the numbers of correctly and incorrectly classified samples broken down by each class. The columns of the matrix represent actual classes, whereas the predicted classes by the classification algorithm are presented in the rows of the matrix. As can be seen in Table 10, confusion matrix reports four cases: the true positive (TP) case, which stands for the correctly identified disease, true negative (TN) case representing the correctly rejected disease and false negative (FN) and false positive (FP) case denoting the first and the second error. Whereas the first type error, predict positive diagnosis while the actual condition is negative, the second type error is considered as the fatal error since the prediction of the disease absence is false. [49]

For the purpose of the final classification two classification models were proposed. The polynomial SVM model, which reached the highest accuracy during the process of optimal SVM model selection, and the artificial neural network model with 4 hidden layers and descending number of neurons in particular layers (specifically, 700-500-300-100). The confusion matrices summarizing all correct and incorrect classifications for both classification models are constructed in Table 10. According to the data presented in this table, the diagonal values of the ANN classification confusion matrix indicate 139 correctly classified cases out of 144, which resulted in an efficiency of 96.53 %. Higher accuracy was reached by the SVM model, with 141 correct classifications out of 144, that gives an efficiency of 97.92 %.

Table 10: Confusion matrices of blood cells identification for the proposed classification models

	SVM Classification		**ANN**	
	Disease positive	Disease negative	Disease positive	Disease negative
Test positive	71	2	70	3
Test negative	1	70	2	69
	Overall Accuracy: 97.92 %		Overall Accuracy: 96.53 %	

There are different evaluation metrics, which can be obtained from the confusion matrix values. The fundamental parameter is the accuracy that is the ratio of the correct prediction. However this metric has limitations in evaluating the performance, especially in minority classes with imbalanced distribution, four other performance measures are used in this thesis. Two of them are sensitivity and specificity, which are defined by the following formulas

$$Sensitivity = \frac{TP}{TP + FN} \tag{49}$$

$$Specificity = \frac{TN}{TN + FP} \tag{50}$$

Sensitivity and specificity reflect early warnings from two different perspectives. While sensitivity, also known as recall, denotes how often the positive results are predicted correctly, specificity measures correct negative predictions. These two measures are inversely proportional, which means, that with the increasing sensitivity decrease the specificity and vice versa. In medical field, reaching 100% value of such a measure is not reasonable. The sensitivity achieving 100 % can be in medical practice reached by just predicting that all patients do not suffer from disease and therefore the test will never commit the second, or the false positive error. Generally, very high specificity is required in cases where the principal goal is to limit the number of false negatives.

Usually sensitivity and specificity values are combined together for the purpose of achieving a better overview of the diagnosis efficiency. This idea is based on the assumptions that a good

predictive model must have a good combination of successful positive predictions as well as successful negative predictions. To take into account both mentioned measures F1 Score metric is introduced. This predictive value is defined as [50]

$$F_1 = \frac{Sensitivity * specificity}{Sensitivity + specificity} = \frac{2TP}{2TP + FP + FN} \quad (51)$$

The last evaluation criteria used in this thesis is called error rate or the misclassification rate, which gives a percent of misclassified samples out of the total samples in the validation data. The definition of the error rate is given as [49]

$$ERR = \frac{FP + FN}{TP + FP + TN + FN} \quad (52)$$

6.2 Overall results

These performance metrics were calculated for both classification methodologies, which allow comparing the selected classification methods in terms of their prediction performance. Table 11 shows the prediction results of the polynomial SVM classification model and selected ANN architecture. The proposed approach, which achieved the highest precision detects leukemic cells in 98.61 % and identifies normal cells with the precision of 97.22 %.

Table 11: Performance measures for the selected supervised classifiers

	Accuracy	Sensitivity	Specificity	F_1	Error Rate
SVM classification	97.92	98.61	97.22	97.93	2.03
ANN	96.53	97.22	95.83	96.55	3.47

The problem of acute leukemia classification that is based solely on the cell morphology has been addressed by several research studies. The comparison of the proposed acute leukemia detection approach with other relevant methodologies, in terms of accuracy is shown in Table 12.

One of the highest accuracy was reached by Pedeira, C.E et al. By applying the mutual information-based methodology and neural network to estimate the presence of the leukemic cells they achieved an accuracy of 98.2 %. Another automatic leukemia detection method was proposed by Moradi Amin et al. in which they deployed histogram equalization and linear contrast stretching for preprocessing and k-mean clustering method for image segmentation. The multi-Support vector machine classifier used for the purpose of blood cell classification in this case is able to detect leukemic cells with the accuracy of 97 %.

In comparison with other studies, Chatap et al. applied different approach, which deployed global thresholding using Otsu threshold technique for leukocyte segmentation. After extracting geometrical features, k nearest neighbor classifier was trained to achieve the total accuracy of 93%.

Table 12: Studies carried out for the normal and leukemic cells classification.

Authors, year	Segmentation	Classifier	Number of images	Accuracy [%]
Pedreira, C.E et al., 2012 [62]	Watershed method, unsupervised color segmentation	ANN	189	98.2
Viswanathan, P. et al.,2015 [63]	Morphological contour based	Fuzzy C means	108	98.0
Dumyan and Gupta, 2017 [64]	Image binarization, Canny edge detection	ANN	36	97.8
Amin, M.M. et al., 2015 [65]	K-means clustering	SVM	312	97.0
Bhattacharjee, R. et al., 2015 [66]	Morphological operators	ANN	120	95.2
Mohapatra and Patra, 2010 [67]	K-means clustering, NN[9]	SVM	108	95.0
Chatap et al., 2014 [68]	Otsu's threshold	K-NN	368	93.0
Putzu, L. et al., 2017 [69]	Zack algorithm	SVM	245	92.0

According the table above, finally it needs to be realized that most authors tested their proposed system with their own data sets, which are not publicly available. Therefore, there is no possibility to directly compare the findings in this thesis with the results obtained by other various proposed leukemic cell detection systems.

[9] Nearest neighbor classifier

7 Software architecture

The architecture of the software is written in accordance with the basic key points of National Instruments and programing techniques. The main idea behind the proposed system is to have an easy code maintenance and management and easy debugging with possibilities of code reuse. The final standpoint of such a solid architecture is the unit testing and execution profiling. Generally, a good software architecture must balance the scalability, modularity, reusability, and extensibility of code while preserving the low complexity.

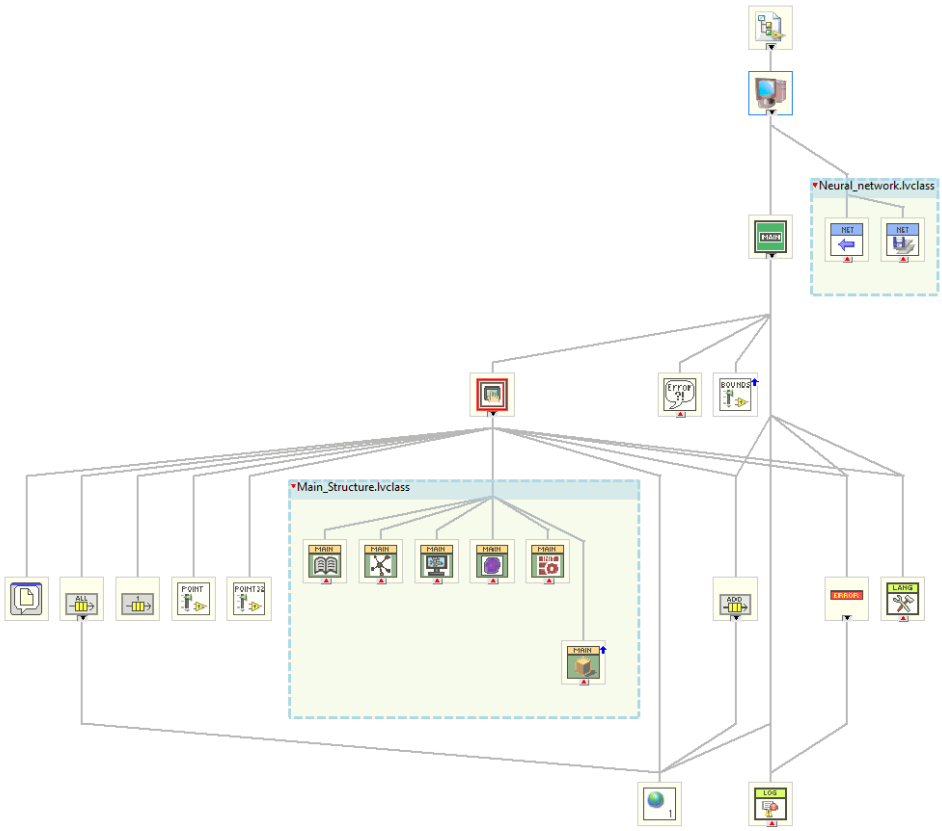

Figure 32: Class hierarchy of the designed application.

To fulfill all standpoints, an objected-oriented programming architecture was used. The particular processing tasks were distributed over separate building blocks from the lowest-level classes, which are self-sufficient and handle the basic image processing tasks, to the top level class. This is a typical top-down design pattern where building blocks, which perform work at the policy level, will delegate behavior down an increasingly detail-focused chain of dependencies. The designed mid-level classes, which form the link between the highest and lowest layers of the application, then contain low-level image processing classes and scale them to a less general purpose but more dedicated solution. The final layer consists of top-level routines, which handle all other classes and support sub-procedures that are built for the specific purpose. Table 13 summarizes the general division of the proposed classes into particular layers.

Table 13: The proposed system of class layouts

	Top-level	Mid-level class	Low-level class
Class name	Main.vi	Main_Structures	Classification
		Neural_Network	Features_Computation
			Segmentation

7.1 Top-level

The top level framework is based on handling a graphical user interfaces together with a functionality of calling the mid-level classes. The top-level layer also handles basic functionality related to debugging purposes, or application interface. This covers utilities for storing logged data and creation of log files on a disk drive, or the language settings of an application.

After the dynamic loading of all modules in the top-level layer, the application is handled by queued event-driven Producer/Consumer in LabVIEW. This design pattern is based on the Master/Slave pattern, and is geared towards enhanced data sharing between multiple loops running at different rates. The Producer/Consumer pattern is broken down into two parallel loops; the first loop which produces data on the basis of the user's actions, and the second loop that consumes the produced data. The synchronization of the loops in this case is ensured by the event handling structure and the communication between the producer and consumer is realized by using data queues. Furthermore using queues offer also the advantage of data buffering between the producer and the consumer loop. The constructed queued event-driven Producer/Consumer design pattern used in the top-level layer is depicted in Figure 33.

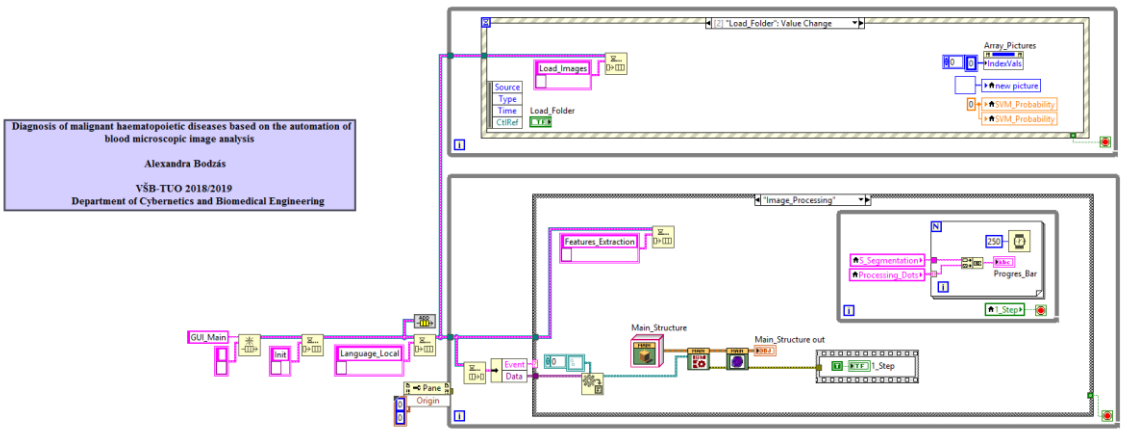

Figure 33: Handling user actions by producer/consumer loops.

Using this pattern lowers the system requirements by stopping a run of the program, whenever there is no real user action. Also by National Instruments suggestions, the data passing form the producer to consumer have a structure containing a string, which denotes the event and binary data corresponding the given data. Thus allows any type of data to be passed in the queue.

7.2 Mid-level

Mid-level is considered to be the core class of the application, which carries all the essential inputs and outputs of the lowest layers. Therefore the main role of the middle level is to assemble the low-level sub-processing blocks. The information between the particular blocks is transferred within the class data references, which allows encapsulation of the program. In fact, encapsulation is a consolidation of data and methods into a class wherein the data are accessible only through class member subroutines. It enables to create modular blocks of code, which can be easily updated or changed without affecting other sections of code within the whole application

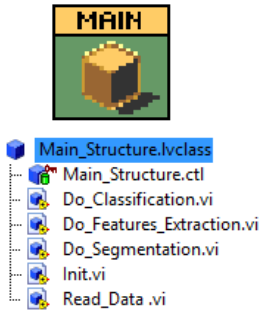

Figure 34: Main_Structure class, connecting the top-level layer with the low-level image processing tasks.

The main class contains five fundamental methods performing the initialization, digital image processing phases and a final method for data member access. The detailed descriptions of particular methods are described in Table 14.

Table 14: Detailed overview of the individual methods of a chosen mid-level class

VI name	Purpose
Init	*Class initialization, which load all images from a folder for the subsequent processing.*
Do segmentation	*Perform the image preprocessing and segmentation task for the purpose of leukocyte extraction. The output of the segmentation block constitutes of several arrays comprising extracted white blood cells and their main cell components (cell nucleus and cytoplasm).*
Do features extraction	*Compute geometrical, 1st order statistical and 2ns order statistical features for each extracted cell or its component. The output of the feature extraction processing block is a 16×N array, where N denotes the number of cells.*
Do classification	*Perform the proposed supervised classification methods based on the trained data on the given features. For a detailed overview see Chapter 7.3.*
Read Data	*Get all classification results.*

7.3 Low–level

Low level classes are the simple "workers" that perform the main processing tasks from the preprocessing of the images to the final classification. Each class corresponds to a separate operation providing the particular image processing phase. These low-level classes are designed in the way, which reflect the functionality of standardized National Instrument drivers. Since all classes use their methods and properties to store the data and produce results for subsequent processing, such programming techniques are used that take into account the modifiability, encapsulation, extensibility and ease of use. All proposed methods of the classification class are demonstrated in Figure 35.

Figure 35: Particular methods of the low-level classification class

- ***1) Get data*** *– get all features obtained by the features computation phase*
- ***2) Data normalization*** *– scales all features in a predetermined range of < 0, 1 >*
- ***3) SVM classification –*** *perform polynomial SVM classification on the given data*
- ***4) ANN classification –*** *perform the classification based on the proposed ANN architecture*
- ***5) Evaluation –*** *evaluation of the final diagnosis and particular numbers of cell types*
- ***6) Read data –*** *get all classification results*

Conclusion

Leukemia is a malignant disease, which is characterized by the rapid and uncontrolled accumulation of abnormal white blood cells. The chances of the positive prognosis solely depend on the early detection and diagnosis of the disease. The primary suspicion of the leukemia is indicated by observing cellular internal structure abnormalities of white blood cells in the peripheral blood smear. This microscopic examination of blood slides is time-consuming process and requires considerable training and experience. Furthermore the examination results often lack standardized protocol and performance owing to a variety of factors such as insufficient expertise, operator fatigue or imperfection of the stained samples. To circumvent the drawbacks of this manual microscopic evaluation of blood smears, an efficient computer aided methodologies are required to be developed. The work presented in this thesis therefore focuses on automated detection of leukemic cells in peripheral microscopic blood smear images on the basis of image processing and machine learning techniques.

The proposed methodology in this thesis involved four main stages, namely image preprocessing, image segmentation, feature extraction and the final classification. The most challenging phase was the segmentation process, which was further divided into two parts; the single white blood cell localization and the extraction of separate cells and their particular regions. For this purpose various image processing techniques such as image thresholding, mathematical morphology or edge detection were combined.

The extracted sub-images of individual cells and their separated cell components (nucleus and cytoplasm) were subsequently used for the feature extraction phase. To differentiate normal and leukemic cells in the microscopic blood smear images, a total of 16 features representing the morphology, texture and other statistical-based information were selected. All selected features mainly aim to extract the information with respect to the cytoplasm size, nucleus size, nucleus shape, amount of cytoplasm, or the structure of nucleus chromatin.

The final classification was conducted using two different methods, the neural network and the support vector machine. To evaluate the proposed algorithm, a dataset comprising 241 segmented white blood cells was used. The designed neural network architecture achieved an overall accuracy of 96.53 %, while the SVM algorithm using the polynomial kernel was able to classify 141 leukocytes correctly out of 144, which has given an efficiency of 97.92 %. In order to evaluate the effectiveness of both classification models, the predicted values were compared with the actual ones by constructing the confusion matrix. The results obtained within the framework of this thesis show that the proposed algorithm achieves an acceptable performance for the detection of leukemic cells presented in peripheral blood smear images.

References

[1] *Blood: Physiology and Circulation*. New York: Britanica Educational Publishing, 2010. ISBN 1615302506.

[2] Blood basics. *American Society of Hematology* [online]. [cit. 2018-09-27]. Retrieved from http://www.hematology.org/Patients/Basics/

[3] BETHESDA, Dean L. *Blood Groups and Red Cell Antigens* [online]. US, 2005 [cit. 2018-09-27]. Retrieved from National Center for Biotechnology Information

[4] ASHTON, Nick. Physiology of red and white blood cells. *Anaesthesia & Intensive Care Medicine* [online]. 2013, **14**(6), 261-266 [cit. 2018-09-27]. Retrieved from https://www.sciencedirect.com/science/article/pii/S1472029913000787

[5] Anatomy and physiology: Leukocytes and Platelets. *BC Open Textbooks* [online]. [cit. 2018-09-27]. Retrieved from https://opentextbc.ca/anatomyandphysiology/chapter/18-4-leukocytes-and-platelets/

[6] JAGANNATHAN-BOGDAN, M. a L. I. ZON. Hematopoiesis. *Development* [online]. 2013, **140**(12), 2463-2467 [cit. 2018-09-27]. DOI: 10.1242/dev.083147. ISSN 0950-1991. Retrieved from http://dev.biologists.org/cgi/doi/10.1242/dev.083147

[7] The International Agency for Research on Cancer. *WHO classification of tumours of haematopoietic and lymphoid tissues*. 4th rev. ed. France: IARC, 2017. ISBN 9789283244943

[8] BAIN, B. J. Routine and specialised techniques in the diagnosis of haematological neoplasms. *Journal of Clinical Pathology* [online]. 1995, (48), 501-508 [cit. 2018-09-27]. Retrieved from https://jcp.bmj.com/content/jclinpath/48/6/501.full.pdf

[9] ADEWOYIN, AS a B. NWOGOH. Peripheral blood film - A review. *Ann Ib Postgrad Med.* [online]. 2014, **12**(2), 71–79 [cit. 2018-09-27]. Retrieved from https://www.ncbi.nlm.nih.gov/pmc/articles/PMC4415389/

[10] FAGUET, Guy B. *Hematologic Malignancies: Methods and Techniques*. 2nd ed. Totova: Humana Press, 2001. ISBN ISBN-13: 978-0896035430.

[11] *Journal of Clinical Pathology* [online]. 1994, **47**(9) [cit. 2018-09-30]. ISSN 0021-9746. Retrieved from http://jcp.bmj.com/cgi/doi/10.1136/jcp.47.9.777

[12] CRAIG, Fiona E. a Kenneth A. FOON. Flow cytometric immunophenotyping for hematologic neoplasms. *Blood* [online]. 2008, (111), 3941-3967 [cit. 2018-09-30]. Retrieved from http://www.bloodjournal.org/content/111/8/3941?sso-checked=true

[13] PRAKASH, Gaurav, Anupriya KAUR, Pankaj MALHOTRA, Alka KHADWAL, Prashant SHARMA, Vikas SURI, Neelam VARMA a Subhash VARMA. Current Role of Genetics in Hematologic Malignancies. *Indian Journal of Hematology and Blood Transfusion* [online]. 2016, **32**(1), 18-31 [cit. 2018-10-05]. DOI: 10.1007/s12288-015-0584-4. ISSN 0971-4502. Retrieved from https://www.ncbi.nlm.nih.gov/pmc/articles/PMC4733682/

[14] LI, Marilyn, Daniel PINKEL, Pankaj MALHOTRA, Alka KHADWAL, Prashant SHARMA, Vikas SURI, Neelam VARMA a Subhash VARMA. Clinical cytogenetics and molecular cytogenetics. *Journal of Zhejiang University SCIENCE B* [online]. 2006, **7**(2), 162-163 [cit. 2018-10-06]. DOI: 10.1631/jzus.2006.B0162. ISSN 1673-1581. Retrieved from https://www.ncbi.nlm.nih.gov/pmc/articles/PMC1363764/

[15] CONRAD STÖPPLER, Melissa. Leukemia. *Medicinenet* [online]. [cit. 2018-09-27]. Retrieved from https://www.medicinenet.com/leukemia/article.htm#leukemia_facts

[16] Acute Myeloid Leukemia (AML) Subtypes and Prognostic Factors. *American Cancer Society [online]. [cit. 27-09-2018]*. Retrieved from https://www.cancer.org/cancer/acute-myeloid-leukemia/detection-diagnosis-staging/how-classified.html

[17] Leukemia - Cancer Stat Facts. Surveillance, Epidemiology, and End Results Program [online]. Retrieved from https://seer.cancer.gov/statfacts/html/leuks.html

[18] Facts and Statistics, *Leukemia and Lymphoma Society*. *Leukemia & Lymphoma Society* [online]. Retrieved from https://www.lls.org/http%3A/llsorg.prod.acquia-sites.com/facts-and-statistics/facts-and-statistics-overview/facts-and-statistics

[19] SADIQ, Muhammad Arif et al. Haematological manifestations and frequency of fab subtypes in patients of acute myeloid leukaemia. *Pak Armed Forces Med J* [online]. 2015, **65**(5), 610-615 [cit. 2018-09-26]. Retrieved from https://www.ejmanager.com/mnstemps/155/155-1459760112.pdf

[20] SMITH, B. Douglas a M. STEIN. Acute myeloid leukemia. *ASH - Self assessement program* [online]. [cit. 2018-09-26]. Retrieved from http://www.ash-sap.org/content/2016/521.extract#cited-by

[21] CASTRO, W.Ladines et al. Morphology of leukaemias. *Revista Médica del Hospital General de México* [online]. 2016, **79**(2), 107-113 [cit. 2018-09-26]. Retrieved from https://www.sciencedirect.com/science/article/pii/S0185106315000724

[22] Signs and Symptoms of Acute Myeloid Leukemia (AML). *Cancer* [online]. [cit. 2018-09-26]. Retrieved from https://www.cancer.org/cancer/acute-myeloid-leukemia/detection-diagnosis-staging/signs-symptoms.html

[23] TERWILLIGER, T a M ABDUL-HAY. Acute lymphoblastic leukemia: a comprehensive review and 2017 update. *Blood Cancer Journal*. 2017, **7**(6). DOI: 10.1038/bcj.2017.53. ISSN 2044-5385. Retrieved from http://www.nature.com/doifinder/10.1038/bcj.2017.53

[24] KATZ, Aaron J., Victoria M. CHIA, Wilma M. SCHOONEN a Michael A. KELSH. Acute lymphoblastic leukemia: an assessment of international incidence, survival, and disease burden. *Blood Cancer Journal*. 2015, **26**(11), 1627-1642. DOI: 10.1007/s10552-015-0657-6. ISSN 0957-5243. Retrieved from http://link.springer.com/10.1007/s10552-015-0657-6

[25] MCCLATCHEY, Kenneth D. *Clinical Laboratory Medicine*. 2nd ed. Philadelphia: Lippincott Williams & Wilkins, 2002. ISBN ISBN-13: 978-0683307511.

[26] NEGRIN, Robert S a Charles A SCHIFFER. Treatment of chronic myeloid leukemia in accelerated phase. *Www.uptodate.com* [online]. 2017 [cit. 2018-09-26]. Retrieved from https://www.uptodate.com/contents/treatment-of-chronic-myeloid-leukemia-in-accelerated-phase

[27] MORRISON, Vicki A. Chronic leukemias. *CA Cancer J Clin* [online]. 1994, **44**, 353-377 [cit. 2018-09-27]. Retrieved from https://onlinelibrary.wiley.com/doi/abs/10.3322/canjclin.44.6.353

[28] *Atlas of Haematological Cytology* [online]. 2016 [cit. 2018-09-26]. Retrieved from http://www.leukemia-cell.org/atlas/index.php?pg=images--myeloproliferative-neoplasms--chronic-myeloid-leukaemia-bcr-abl1-positive--blast-phase--myeloblastic-crisis#1

[29] Chronic lymphocytic leukemia (CLL), B-cell. *Pathpedia* [online]. [cit. 2018-09-26]. Retrieved from https://www.pathpedia.com/education/eatlas/histopathology/blood_cells/chronic_lymphocytic_leukemia_(cll)_b-cell.aspx

[30] OPENCV TEAM. About. *Opencv* [online]. [cit. 2018-10-16]. Retrieved from https://opencv.org/about.html

[31] Image Processing Toolbox: Perform Image Processing, Analysis, and Algorithm Development. *Mathworks*[online]. [cit. 2018-10-16]. Retrieved from https://www.mathworks.com/products/image.html

[32] BITTER, Rick, Taqi MOHIUDDIN a Matt NAWROCKI. *LabView advanced programming techniques*. 2nd ed. Boca Raton, FL, c2007. ISBN 978-084-9333-255.

[33] LabVIEW Object-Oriented Programming FAQ. *Ni* [online]. 2014 [cit. 2018-10-16]. Retrieved from http://www.ni.com/white-paper/3573/en/

[34] NATIONAL INSTRUMENTS. *Vision Development Module for LabVIEW, LabWindows/CVI, and Measurement Studio* [online]. [cit. 2018-10-16]. Retrieved from https://pdfs.semanticscholar.org/presentation/22f7/79667956c413b84505947d4857c237ed4135.pdf

[35] SEBE, Nicu a Michael S LEW. *Robust computer vision: theory and applications*. Boston: Kluwer Academic, c2003. ISBN 14-020-1293-4.

[36] GONZALEZ, Rafael C a Richard E WOODS. *Digital image processing: theory and applications*. 3rd ed. Upper Saddle River, N.J.: Prentice Hall, c2008. ISBN 978-0-13-168728-8.

[37] SOJKA, Eduard, Jan GAURA a Michal KRUMNIKL. *Matematické základy digitálního zpracování obrazu* [online]. 2011 [cit. 2018-10-23]. Retrieved from http://mrl.cs.vsb.cz//people/sojka/dzo/mzdzo.pdf

[38] FRERY, Alejandro C a Talita PERCIANO. *Introduction to image processing using R: learning by examples*. New York: Springer, [2013]. SpringerBriefs in computer science.

[39] ČADÍK, Martin. Perceptual Evaluation of Color-to-Grayscale Image Conversions. *Computer Graphics Forum*. 2008, **27**(7), 1745-1754.

[40] BURGER, Wilhelm. *Digital image processing: an algorithmic introduction using Java*. New York: Springer, c2008. ISBN 978-1-84628-379-6.

[41] SRISHA, Ravi & Khan, Am. *Morphological Operations for Image Processing: Understanding and its Applications* [online]. 2013, , 17-19 [cit. 2018-12-03]. Retrieved from https://www.researchgate.net/publication/272484795_Morphological_Operations_for_Image_Processing_Understanding_and_its_Applications

[42] RAJIV, RajivKumar a A. M. ARTHANARIEE. A Comparative Study of Image Segmentation Using Edge-Based Approach. *International Journal of Mathematical and Computational Sciences*. 2013, **7**(3).

[43] PLATANIOTIS, Konstantinos N a A. N VENETSANOPOULOS. *Color image processing and applications*. New York: Springer, c2000. Digital signal processing (Springer-Verlag). ISBN 35-406-6953-1.

[44] AHMED, Alaa Shakir, Dr. M. MORSY, Mohy Eldin A. ABO-ELSOUD a E.S. COSTA. Microscopic Digital Image Segmentation And feature Extraction of Acute Leukemia. *International Journal of Science and Engineering Applications* [online]. Singapore: Springer Singapore, 2016, 2016-02-26, **5**(5), 228-233 [cit. 2019-04-19]. Advances in Intelligent Systems and Computing. DOI: 10.7753/IJSEA0505.1001. ISBN 978-981-10-0133-8. ISSN 23197560. Retrieved from http://www.ijsea.com/archive/volume5/issue5/IJSEA05051001.pdf

[45] CHATHURANGI, Shyalika. Feature Extraction in Leukemia Diagnosis using Image Analysis. *Medium.com*[online]. Dec 9,2017 [cit. 2019-04-19]. Retrieved from https://medium.com/@chathurangijks/feature-extraction-in-leukemia-diagnosis-using-image-analysis-46243c3f66fa

[46] BATCHELOR, Bruce G. a Frederick M. WALTZ. *Intelligent machine vision: techniques, implementations, and applications*. New York: Springer, c2001. ISBN 978-3-540-76224-9.

[47] HENRY, William, Dr. M. MORSY, Mohy Eldin A. ABO-ELSOUD a E.S. COSTA. Texture Analysis Methods for Medical Image Characterisation. *Biomedical Imaging* [online]. Singapore: InTech, 2010, 2010-03-01, **5**(5), 228-233 [cit. 2019-04-19]. Advances in Intelligent Systems and Computing. DOI: 10.5772/8912. ISBN 978-953-307-071-1. ISSN 23197560. Retrieved from http://www.intechopen.com/books/biomedical-imaging/texture-analysis-methods-for-medical-image-characterisation

[48] RASCHKA, Sebastian. About Feature Scaling and Normalization: – and the effect of standardization for machine learning algorithms. *Sebastianraschka.com* [online]. [cit. 2019-04-19]. Retrieved from https://sebastianraschka.com/Articles/2014_about_feature_scaling.html

[49] Basic evaluation measures from the confusion matrix. *Classeval.wordpress.com* [online]. [cit. 2019-04-19]. Retrieved from https://classeval.wordpress.com/introduction/basic-evaluation-measures/

[50] Confusion Matrix. *Skymind.ai* [online]. [cit. 2019-04-19]. Retrieved from https://skymind.ai/wiki/accuracy-precision-recall-f1

[51] FRADKIN, Dmitriy a Ilya MUCHNIK. *Support Vector Machines for Classication* [online]. 2006 [cit. 2019-04-20]. Retrieved from https://www.researchgate.net/publication/242386967_Support_Vector_Machines_for_Classication

[52] SAYAD, Dr. Saed. Support Vector Machine - Classification (SVM). *Www.saedsayad.com* [online]. [cit. 2019-04-19]. Retrieved from https://www.saedsayad.com/support_vector_machine.htm

[53] HALTUF, Michal. *Support Vector Machines for Credit Scoring*. Prague, 2014. Master thesis. University of Economics. Supervisor Doc. RNDr. Jiří Witzany, Ph.D.

[54] Support Vector Machines. *Zone.ni.com* [online]. 2016 [cit. 2019-04-20]. Retrieved from https://zone.ni.com/reference/en-XX/help/370281AC-01/nivisionconcepts/supportvectormachines/

[55] NIELSEN, Michael. Using neural nets to recognize handwritten digits. *Neuralnetworksanddeeplearning.com* [online]. Oct, 2018 [cit. 2019-04-20]. Retrieved from http://neuralnetworksanddeeplearning.com/chap1.html

[56] AGATONOVIC-KUSTRIN, S a R BERESFORD. Basic concepts of artificial neural network (ANN) modeling and its application in pharmaceutical research. Journal of Pharmaceutical and Biomedical Analysis[online]. 2000, 22(5), 717-727 [cit. 2019-04-20]. DOI: 10.1016/S0731-

7085(99)00272-1. ISSN 07317085. Retrieved from https://linkinghub.elsevier.com/retrieve/pii/S0731708599002721

[57] SAXENA, Shubh. Artificial Neuron Networks(Basics): Introduction to Neural Networks. Becominghuman.ai[online]. Oct 26,2017 [cit. 2019-04-20]. Retrieved from https://becominghuman.ai/artificial-neuron-networks-basics-introduction-to-neural-networks-3082f1dcca8c

[58] Convolutional neural network: Building blocks. En.wikipedia.org [online]. [cit. 2019-04-20]. Retrieved from https://en.wikipedia.org/wiki/Convolutional_neural_network

[59] Neural Networks & The Backpropagation Algorithm, Explained: Neurons, as an Extension of the Perceptron Model. *Jeremykun.com* [online]. December 9, 2012 [cit. 2019-04-20]. Retrieved from https://jeremykun.com/2012/12/09/neural-networks-and-backpropagation/

[60] KAPUR, Rohan. Neural Networks & The Backpropagation Algorithm, Explained: https://ayearofai.com/rohan-lenny-1-neural-networks-the-backpropagation-algorithm-explained-abf4609d4f9d. *Ayearofai.com* [online]. March 3, 2016 [cit. 2019-04-20]. Retrieved from https://jeremykun.com/2012/12/09/neural-networks-and-backpropagation/

[61] SURYANSH, S. Gradient Descent: All You Need to Know: Gradient Descent is THE most used learning algorithm in Machine Learning and this post will show you almost everything you need to know about it. *Hackernoon.com* [online]. March 12, 2018 [cit. 2019-04-20]. Retrieved from https://hackernoon.com/gradient-descent-aynk-7cbe95a778da

[62] PEDREIRA, C.E., L. MACRINI, M.G. LAND a E.S. COSTA. New Decision Support Tool for Treatment Intensity Choice in Childhood Acute Lymphoblastic Leukemia. *IEEE Transactions on Information Technology in Biomedicine* [online]. 2009, **13**(3), 284-290 [cit. 2019-04-19]. DOI: 10.1109/TITB.2008.925965. ISSN 1089-7771. Retrieved from http://ieeexplore.ieee.org/document/4526693/

[63] *Procedia Computer Science* [online]. 2015, **58**(3) [cit. 2019-04-19]. ISSN 18770509. Retrieved from https://linkinghub.elsevier.com/retrieve/pii/S1877050915021286

[64] DUMYAN, Savita, A. G. An enhanced technique for lymphoblastic cancer detection using artificial neural network. *International Journal of Advanced Research in Computer Science and Electronics Engineering (IJARCSEE)* 2017,6(4),38-42

[65] AMIN MM, KERMANI S, TALEBI A, OGHLI MG. Recognition ofacute lymphoblastic leukemia cells in microscopic imagesusing k-means clustering and support vector machineclassifier. J Med Signal Sens 2015;5(January (1)):49.

[66] BHATTACHARJEE, Romel, Lalit Mohan SAINI, M.G. LAND a E.S. COSTA. Robust technique for the detection of Acute Lymphoblastic Leukemia. *2015 IEEE Power, Communication and Information Technology Conference (PCITC)* [online]. IEEE, 2015, 2015, **58**(3), 657-662 [cit. 2019-04-19]. DOI: 10.1109/PCITC.2015.7438079. ISBN 978-1-4799-7455-9. ISSN 18770509. Retrieved from http://ieeexplore.ieee.org/document/7438079/

[67] MOHAPATRA, S., Patra, D. Automated cell nucleus segmentation and acute leukemia detection in blood microscopic images. Proceedings of the International Conference on Systems in Medicine and Biology, ICSMB 2010; December 2010; India. pp. 49–54.

[68] CHATAP N, SHIBU S. Analysis of blood samples for counting leukemia cells using support vector machine and nearest neighbour. IOSR J Comput Eng. 2014;16(5):79–87.

[69] PUTZU, Lorenzo, Giovanni CAOCCI, Cecilia DI RUBERTO a E.S. COSTA. Leucocyte classification for leukaemia detection using image processing techniques. *Artificial Intelligence in Medicine* [online]. Singapore: Springer Singapore, 2014, 2016-02-26, **62**(3), 179-191 [cit. 2019-04-19]. Advances in Intelligent Systems and Computing. DOI: 10.1016/j.artmed.2014.09.002. ISBN 978-981-10-0133-8. ISSN 09333657. Retrieved from https://linkinghub.elsevier.com/retrieve/pii/S0933365714001031

Image References

[*1*] CellaVision, *Leukocytes in Peripheral Blood* [ONLINE]. Available at: https://www.cellavision.com/en/cellavision-cellatlas/leukocytes [Accessed 18 October 2018]

[*2*] Index of anatomy images [ONLINE]. Available at:http://www.codex99.com/anatomy/images/sturm/sturm_1_lg.jpg [Accessed 18 October 2018]

[*3*] The University of Utah, (2018), *Normal basophil on smear, microscopic* [ONLINE]. Available at: https://library.med.utah.edu/WebPath/HEMEHTML/HEME005.html [Accessed 18 October 2018]

[4] The University of Utah, (2018), Acute myeloblastic leukemia on smear, microscopic [ONLINE]. Available at: https://library.med.utah.edu/WebPath/HEMEHTML/HEME020.html [Accessed 18 October 2018]

[5] The University of Utah, (2018), Chronic myelogenous leukemia on smear, microscopic [ONLINE]. Available at: https://library.med.utah.edu/WebPath/HEMEHTML/HEME022.html [Accessed 18 October 2018]

[6] Shannon McGlauflin, Jolene Munger, and Rebecca Nelson, (2015), Chronic Lymphocytic Leukemia[ONLINE]. Available at: http://rebeccanelson.com/leukemia/cll.html [Accessed 16 October 2018]

[7] Commons.wikimedia.org, (2015), RGB color cube [ONLINE]. Available at: https://commons.wikimedia.org/wiki/File:RGB_color_cube.svg [Accessed 25 April 2019].

[8] Commons.wikimedia.org, (2008), CMYK farbwuerfel [ONLINE]. Available at: https://commons.wikimedia.org/wiki/File:CMYK_farbwuerfel.svg [Accessed 25 April 2019].

[9] Commons.wikimedia.org, (2005), HSV cone [ONLINE]. Available at: https://commons.wikimedia.org/wiki/File:HSV_cone.jpg [Accessed 25 April 2019].

[10] SOJKA, Eduard, Jan GAURA a Michal KRUMNIKL. Matematické základy digitálního zpracování obrazu [online]. 2011 [cit. 2018-10-23]. Retrieved from http://mrl.cs.vsb.cz//people/sojka/dzo/mzdzo.pdf

[11] Saed Sayad, Support Vector Machine - Classification (SVM) [ONLINE]. Available at: https://www.saedsayad.com/support_vector_machine.htm [Accessed 25 April 2019].

[12] Drew Wilimitis, (2018), The Kernel Trick in Support Vector Classification [ONLINE]. Available at: https://towardsdatascience.com/the-kernel-trick-c98cdbcaeb3f [Accessed 25 April 2019].

[13] Wikibooks.org, (2018), Artificial Neural Networks/Activation Functions [ONLINE]. Available at: https://en.wikibooks.org/wiki/Artificial_Neural_Networks/Activation_Functions [Accessed 25 April 2019].

[14] Michael Nielsen, (2018), sigmoid function, step function [ONLINE]. Available at: http://neuralnetworksanddeeplearning.com/chap1.html [Accessed 25 April 2019].

List of annexes

Annex I

BOD0027_Diagnosis_of_Malignant_Haematopoietic_Diseases_based_on_the_Automation_of_Blood_Microscopic_Image_Analysis.rar

(Source code of the application created in the development environment LabVIEW.)